JOURNAL OF GEOPHYSICAL RESEARCH, VOL. 103, NO. A11, PAGES 26,433-26,452, NOVEMBER 1, 1998

Substorm modeling based on observations of an intense high-latitude absorption surge event

Peter Stauning

Danish Meteorological Institute, Copenhagen

Abstract. During the early November 1993 study interval selected for the international Space Weather Initiative a remarkably intense early evening substorm event was observed at around 2200 UT on November 4, 1993, in high-latitude magnetometer and riometer recordings. The event, the most intense absorption event recorded by the imaging riometer in Sdr. Strømfjord (STF), Greenland, during 1993, occurred at the center of strong upward region 1 field-aligned currents during a major reconfiguration of the polar ionospheric plasma convection system. The event was preceded by some substorm activity at lower latitudes. At STF, however, it appeared with nicely isolated and exceptionally clear signatures in the geophysical observations, primarily in the imaging riometer measurements of ionospheric radio wave absorption at 38 MHz. The event was characterized by multiple intense and sudden absorption pulsations with increasing amplitudes of up to 11 dB separated by about 20-30 s and with duration of around 10-15 s superimposed on a general level of a few decibels of absorption. The event was selected for a modeling study to investigate the possible generation mechanisms for the ionized layers causing the absorption. We conclude that the event was most probably caused by precipitation of magnetospheric electrons accelerated repeatedly through transient field-aligned potential structures of 10-30 kV associated with the intense upward currents. We find that these structures were located at a few Earth radii's distance and that the field-aligned potential structures have positive feed-back to the ionospheric potentials affected by the conductivity changes caused by accelerated electrons. We suggest that such coupled potential systems may provide a general mechanism for acceleration of electrons of a thermal magnetospheric plasma to the much higher energies found in auroral precipitation and in the radiation belts.

1. Introduction

The onset of substorms as seen in the explosive brightening of the aurora and the sudden development of magnetic bays and ionospheric absorption events [*Akasofu*, 1964] is one of the most fascinating features of the geophysical environment of the Earth and is still poorly understood in spite of numerous efforts to explain their dramatic and sudden appearance [see, e.g., *Rostoker*, 1972; *McPherron et al.*, 1973; *Pudovkin*, 1991; *Feldstein*, 1991; *Murphree and Cogger*, 1992; *Birn and Hesse*, 1992; *Lui*, 1992; *Lysak et al.*, 1992; *Kan*, 1993; *Kan and Sun*, 1996]. One of the most intriguing problem is that of the timing involved in what appears to be a global phenomena controlled by the interactions of the ionospheric and magnetospheric regions separated by distances of tens to hundreds of thousands of kilometers. The communication of plasma particles or electrical signals between the two regions, which may take minutes, would appear to be a serious constraint for the onset phenomena that can be seen to vary on a scale of a few seconds in the ionosphere following redistributions in the outer magnetosphere.

An explanation of this discrepancy is offered by models which invoke the development near the ionosphere of large field-aligned potential structures that could accelerate the magnetospheric plasma particles to generate the sudden and highly variable energetic auroral particle radiation observed during ionospheric substorms. Such models are supported by numerous observations from rockets and satellites of spectra of precipitated particles with a pronounced peak at some energy in the 1 to 10 keV range that could be explained by a corresponding field-aligned potential drop [e.g., *McIllwain*, 1960; *Hoffman and Evans*, 1968; *Evans*, 1968, 1974].

Magnetospheric field lines are usually considered to be equipotentials since the conductivities along the field are much higher than across. It has been suggested [e.g., *Kindel and Kennel*, 1971] that this assumption can be violated in cases where unstable plasma waves driven by field-aligned currents would interact with the plasma particles to cause anomalous resistivity. The enhanced resistivity would then lead to the buildup of field-aligned potential structures independent of the current flow direction, whether upward or downward. Another possibility which, however, extend only to upward currents, is offered by the limited supply of electrons from the magnetospheric regions to sustain the currents carried downward along the converging auroral field lines by these electrons. Current-voltage relations applicable to field lines in auroral regions have been proposed, among others, by *Knight* [1973], *Lemaire and Scherer* [1974], *Fridman and Lemaire* [1980], *Lyons* [1980, 1992], *Weimer et al.* [1987], *Lu et al.* [1991], and *Pierrard* [1996].

A further element to be considered is the possible feedback effect from the ionosphere when exposed to the precipitating particles accelerated through a field-aligned potential [e.g., *Kan*

Paper number 97JA03596.
0148-0227/98/97JA-03596$09.00

et al., 1984; *Rothwell et al.*, 1984; *Kan et al.*, 1988]. At the start of an event the energetic particle precipitation would cause enhanced ionospheric conductivities and increasing horizontal currents that may further enhance the field-aligned current, thus increasing the potential drop in a fast growing mode. The corresponding effects in a reversed sequence would also make the event decay equally fast. This mechanism was suggested by *Stauning and Rosenberg* [1996] to explain the appearance of dayside absorption spike events in riometer observations near the afternoon convection reversal region.

The present study analyzes an extremely intense substorm absorption event that occurred at ~2156-2206 UT on November 4, 1993, in the high-latitude evening sector within a region of strong upward field-aligned currents near the midnight edge of the convection reversal boundary. The event was preceded by substorm activity at lower latitudes in the midnight sector but formed a strong and isolated event in a region well equipped with observing instruments capable of resolving its temporal and spatial structures. Furthermore, the general polar convection patterns were very well illustrated as a result of the international collaboration, supported by the Space Weather Initiative, to collect and share comprehensive sets of geomagnetic data using, among others, the Assimilative Mapping of Ionospheric Electrodynamics (AMIE) technique for their processing and display. This event therefore is considered well suited for an attempt to model the important mechanisms that may be responsible for the explosive appearance of substorm onsets. A similar event was reported by *Imhof et al.* [1984] using coordinated observations from satellite and ground of an intense electron precipitation spike over the southern polar cap. However, the observational coverage of the conditions within the region of importance was not as complete then as it has been for the present case, and the reported spatial and temporal structures of their event are more unclear. The type of event studied here may also have bearings to the auroral spike events reported, for example, by *Nielsen and Axford* [1977], *Hargreaves et al.* [1979], and *Nielsen* [1980]. In addition to these special events it seems quite possible that the observed features and the suggested mechanisms are important processes of the general substorm scenario.

2. Instrumentation

The Danish Meteorological Institute (DMI) conducts various polar observations related to solar-terrestrial investigations. In Greenland, DMI operates three magnetic observatories equipped with high-precision magnetometers for long-term observations of the Earths main magnetic field supplemented by a number of temporary observing stations. Data sampling is generally at 20-s intervals. Additional MAGIC (Magnetometer Array at Greenland Ice Cap) magnetometers are operated at stations on the Greenlandic ice cap by the University of Michigan in collaboration with DMI. For these instruments the sampling intervals are 15 s. The location of the magnetometer stations are given in Table 1. In addition to defining their coordinates, Table 1 presents the acronyms used for the various stations. Table 1 also lists the invariant latitudes for the stations.

In addition to the magnetometer stations, DMI operates in Greenland a net of normal-beam, standard riometers and two imaging riometers. One in STF (in Greenlandic: Kangerlussuaq, in Danish: Sdr. Strømfjord, in English: Sondrestrom), where the imaging riometer is operated through a collaboration with Institute for Physical Science and Technology at the University of Maryland. The other in Danmarkshavn, where the operation of the IRIS instrument is part of a cooperation with the National Institute of Polar Research in Tokyo. The sampling interval for the standard riometers is 10 or 20 s. For the imaging instruments a complete scan over all channels (beams) is made every 1 s. The imaging riometer for ionospheric studies (IRIS) technique and data handling is explained by *Detrick and Rosenberg* [1990]. The projection of the IRIS beams to ionospheric altitude (90 km) is displayed in their Figure 6. The IRIS instrument in STF has 49 beams, while that in DMH (Danmarkshavn) has 64 beam directions. These beams span an ionospheric area of around 240x240 km (at 90-km reference altitude) with a spatial resolution (pixel size) of around 20 km in the central part. Both these sites have DMI magnetometers, and their locations are given in Table 1.

Table 1. Geomagnetic Observatories in Greenland, November 1993

Station		Geographic Coordinates		Invariant Latitude
Name	Acronym	°N	°E	°N
		West Coast Stations		
Thule	THL	77.47	290.77	85.55
Savissivik	SVS	76.02	294.90	83.80
Kullorsuaq	KUV	74.57	302.82	81.38
Upernavik	UPN	72.78	303.85	79.68
Ummannaq	UMQ	70.68	307.87	77.15
Godhavn	GDH	69.25	306.47	76.12
Attu	ATU	67.93	306.43	74.90
Sdr.Strømfjord	STF	66.99	309.05	73.60
Sukkertoppen	SKT	65.42	307.10	72.43
Godthåb	GHB	64.17	308.27	71.03
Frederikshåb	FHB	62.00	310.32	68.53
Narsarsuaq	NAQ	61.16	314.56	66.86
		Ice Cap Station		
Magic East	MCE	72.34	327.46	75.34
		East Coast Stations		
Nord	NRD	81.60	343.33	80.92
Danmarkshavn	DMH	76.77	341.37	77.29
Daneborg	DNB	74.30	339.78	75.30
Scoresbysund	SCO	70.48	338.03	71.91
Ammagssalik	AMK	65.60	322.37	69.75

The locations of the above stations are illustrated in Figure 1 of Greenland mapped in geographical coordinates. Contours of constant invariant latitude have been included. The location of magnetometer stations are indicated by "dots," while for the imaging riometer system in STF the IRIS beam projections to 90-km reference altitude are indicated in correct scale and orientation. In addition to the observations from the above densely spaced net of observatories located in the region of particular interest for the substorm event studied here, we have also used geomagnetic data from more than 80 stations to define the general polar ionospheric convection patterns. The contributions from these observatories are listed and acknowledged in [Knipp et al., this issue].

3. Substorm Observations

During the selected primary study interval: November 3-5, 1993, for the Space Weather Initiative and following the storm sudden commencement (SSC) at ~1725 UT on November 3, 1993, we see strong substorm activity in the Greenland magnetometer and riometer data starting at 2220 UT on November 3 and

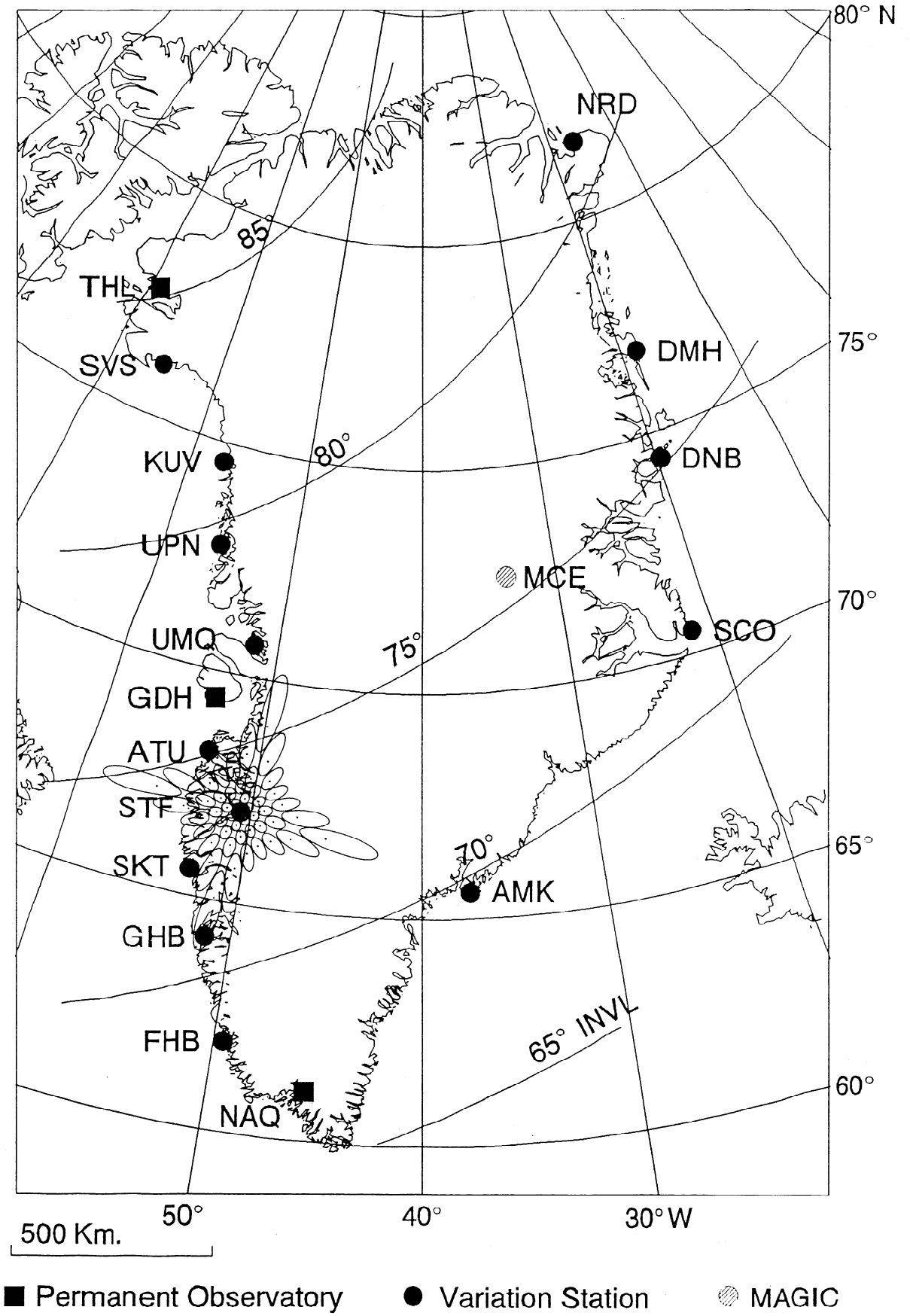

Figure 1. Location of Greenland magnetometer and riometer stations. Projection of IRIS beams to 90 km altitude for imaging riometer in Sdr. Strømfjord.

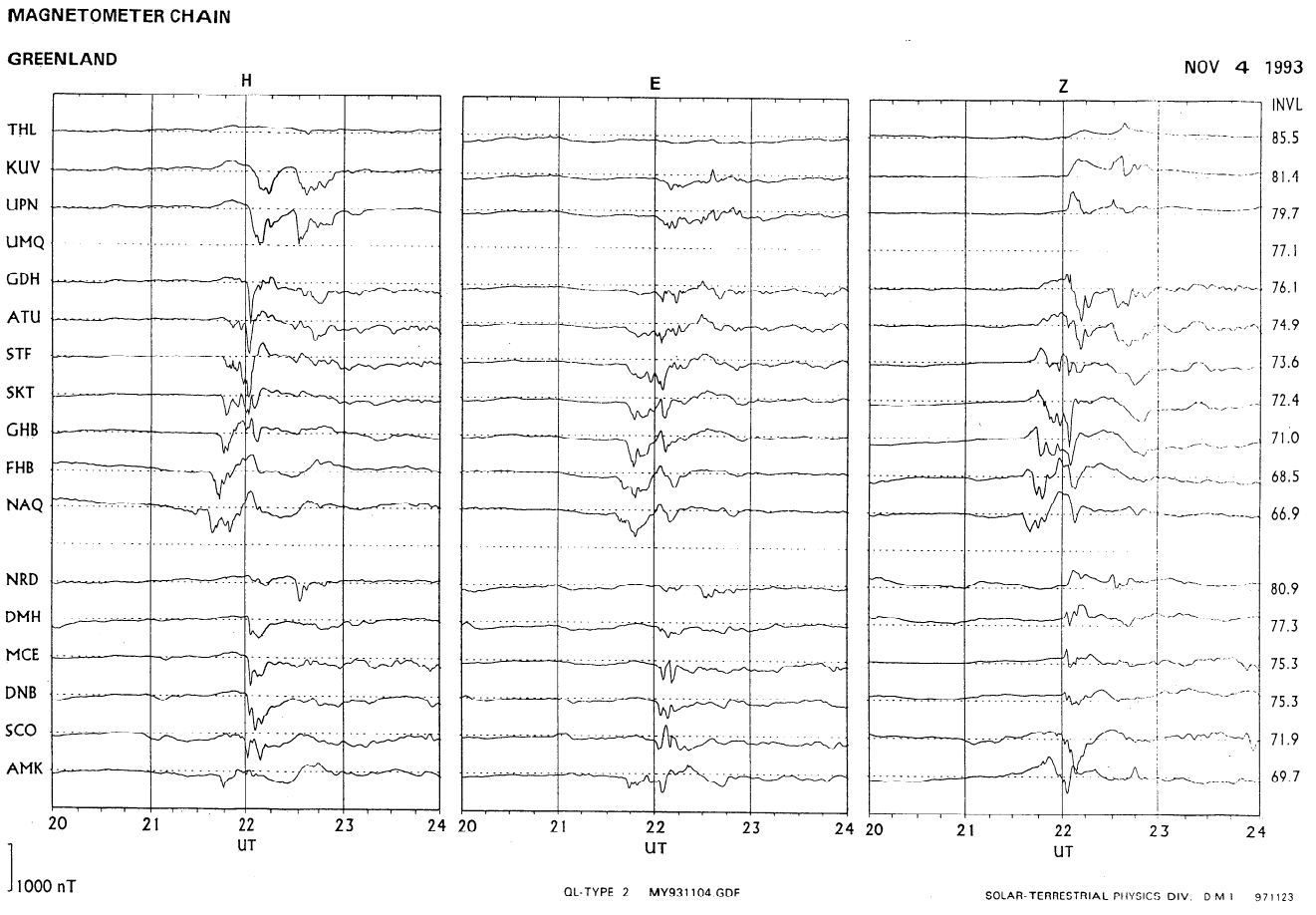

Figure 2. Geomagnetic observations from Greenland during 1800-2400 UT on November 4, 1993. Horizontal northward (H), eastward (E), and downward (Z) components.

continuing at intervals of a couple of hours throughout the storm period. The most disturbed day in the high-latitude regions, for instance STF, is November 5, 1993. However, the most intense absorption event observed from Greenland during this interval occurred during the early evening substorm on November 4, 1993, at around 2156-2206 UT. This substorm, during which the ionospheric absorption of penetrating cosmic noise radio signals reached almost 15 dB at 38 MHz, was also the most intense event observed by the IRIS instruments in Greenland during 1993. The event is analyzed in further detail below.

For the time interval 2000-2400 UT on the selected day, November 4, 1993, the general activity level is displayed in the Greenland magnetometer data presented in Figure 2, which shows the horizontal northward (H), the eastward (E), and the downward (Z) magnetic components. Station acronyms are listed to the left while their invariant latitudes are listed to the right of the diagram for each set of traces. The traces have been divided into two groups with those from the stations NAQ (Narsarsuaq) to THL (Thule) located at the west coast of Greenland displayed in the upper sections of the panels while those from AMK (Ammasalik) to NRD (Nord) from the east coast and MCE (Magic East) from the ice cap are displayed in the lower. Within each group the traces have been arranged according to invariant latitudes. The undisturbed (QL) levels for the displayed components have been marked by the dashed horizontal lines. For the east coast stations magnetic local time is close to universal time, while for the west coast stations the magnetic local time lags universal time by 2 hours. Hence the data displayed in Figure 2 represent the evening to midnight sector in magnetic local time (MLT).

During 2000 to 2130 UT, the level of magnetic activity seen in Figure 2 is generally rather low except for the gradual development of negative deflections in the H components recorded at the southernmost stations AMK, NAQ, and FHB (Frederikshaab) located at auroral zone latitudes. At 2130 UT the sudden and steep onset of a magnetic bay is seen in AMK and NAQ, while a positive bay develops at the northernmost stations, GDH (Godhavn) to THL at the west coast, and DNB (Daneborg) to NRD at the east coast. The region of negative deflection in the H component, which indicate the presence of westward ionospheric currents (eastward plasma flow), expands poleward and arrives at STF at 2143 UT. The current system progresses further poleward to ATU (Attu) and weakens.

Then, around 2200 UT, a new enhancement appear to start at the latitude of STF and to expand further poleward to GDH (Godhavn) as well as equatorward to SKT (Sukkertoppen) and GHB (Godthaab). This is the event to be further investigated in the following.

The variable polar ionospheric convection, which is the dominant cause of the geomagnetic perturbations displayed in Figure 2, is conveniently presented by the polar potential patterns generated through the AMIE technique [*Richmond and Kamide*, 1988]. A sequence of such AMIE potential patterns is displayed in Figure 3 for the very active interval from 2152 to

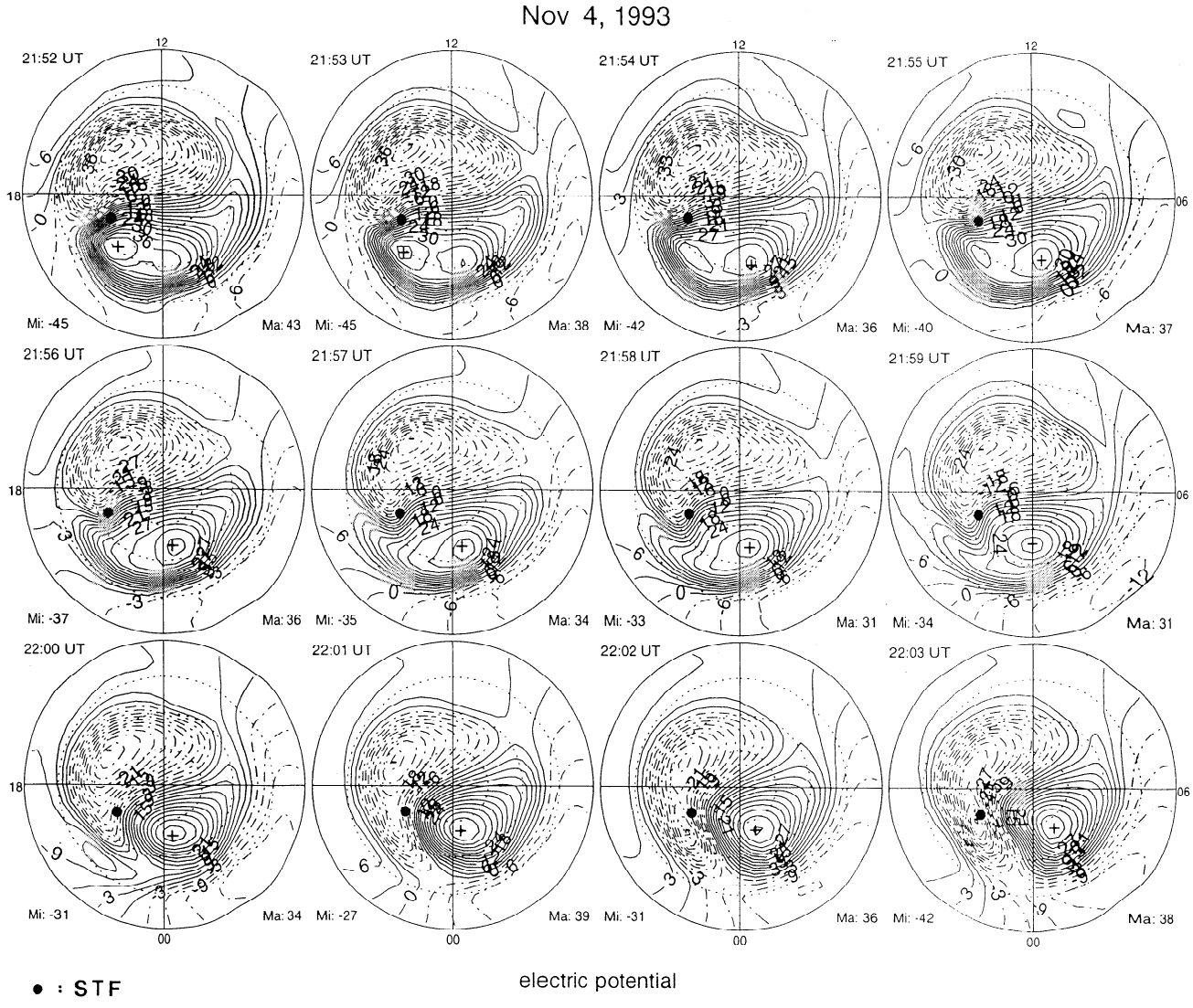

Figure 3. Sequence of AMIE potential plots for the northern polar cap at 1-min interval from 2152 to 2203 UT on November 4, 1993. Outer circle is 55° magnetic latitude. Increment at contour lines is 3 kV.

2203 UT on November 4, 1993. These plots have been generated on basis of magnetometer data from more than 80 stations in polar regions. The magnetometer data have been processed by P. Ernstrøm (DMI, private communication, 1997). To derive the potential patterns, one needs the distributions of the integrated Hall and Pedersen conductivities over the polar cap. The dayside distribution of conductivities is mainly determined through the contribution from the solar illuminated *E* region, which can be modeled to a fair degree [e.g., *Brekke and Moen*, 1993]. At the nightside there are often major contributions from the strongly variable energetic particle precipitation. Here this part has been derived from a conductivity model based on the actual level of magnetic activity [*Ahn et al.*, 1983, 1986].

Each field of Figure 3 presents the instantaneous potential pattern of the northern polar ionosphere in a map of corrected geomagnetic (CGM) latitude (approximately equivalent to invariant latitude) and magnetic local time. The outer circle (solid line) defines 55° magnetic latitude. The dotted circles represent 60°, 70°, and 80° CGM latitudes. Geomagnetic local noon is upward from the pole. The position of STF has been marked by a dot at (73.7°,~19.7 MLT). The potential contours, which are also approximate flow lines for the ionospheric plasma convection, have been computed at one minute intervals from 2152 through 2203 UT to present the temporal development of the convection patterns.

It is seen that the variable patterns depict a dynamical two-cell convection system. At 2153 UT the one (afternoon) cell is located entirely in the day sector while the other (morning) cell occupies the night sector such that the transpolar flow is east-west oriented. At 2203 UT, 10 min later, the two cells have moved closer to their usual positions in the afternoon and morning sectors, respectively, and the transpolar flow is now noon-midnight oriented. It is seen that the development is most rapid during the time interval between 2158 and 2203 UT. Also note that there is some indication that the centers of the convection cells "jumps" to new positions rather than moving continuously. At 2153 UT the primary positive center is located at 2100 MLT, while a second positive center is formed postmidnight at around 0100 MLT in the morning cell. This latter center is subsequently intensified to become dominant after 2155 UT.

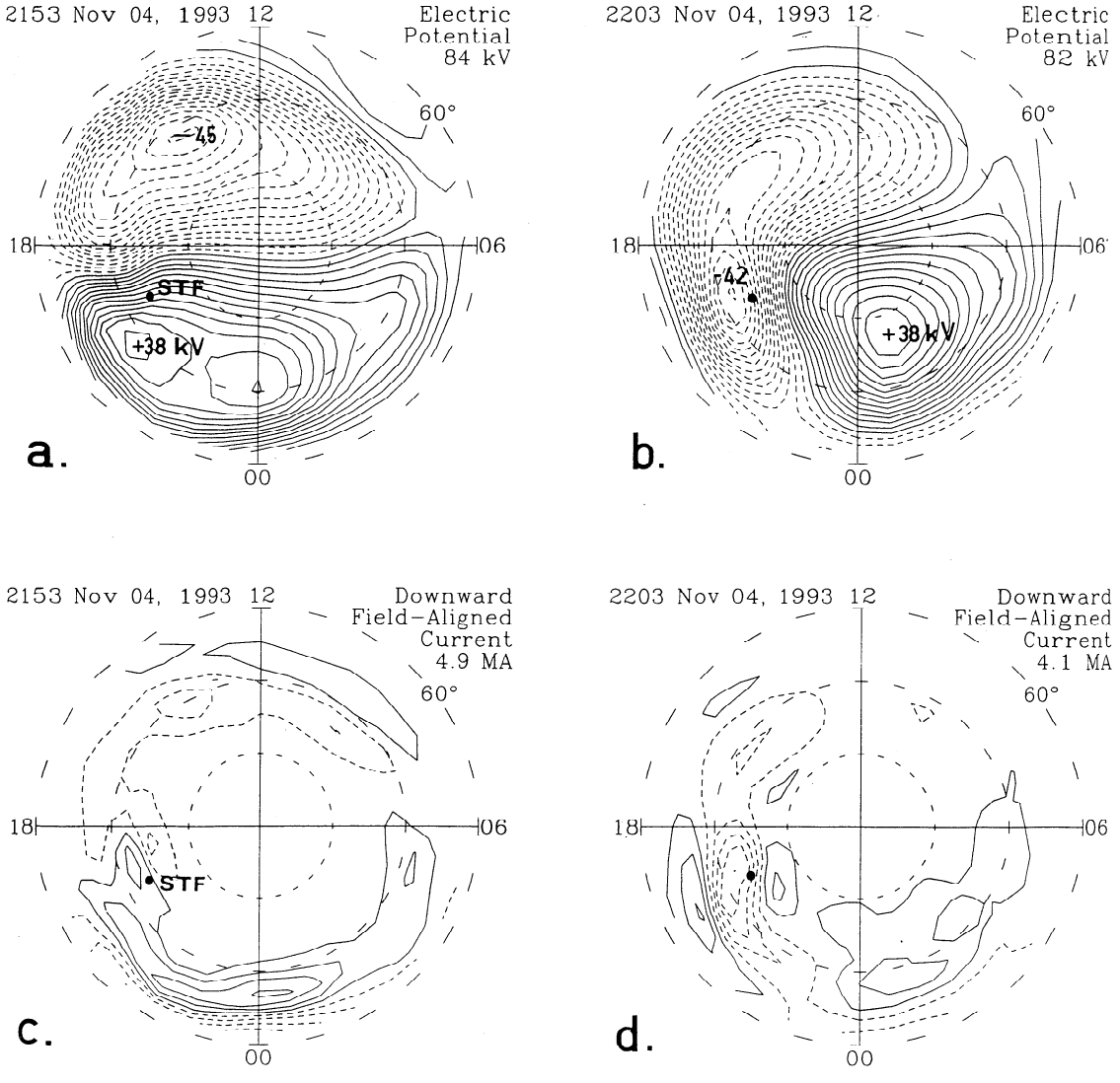

Figure 4. Selected AMIE potential plots for (a) 2153 and (b) 2203 UT on November 4, 1993. Corresponding field-aligned current intensity plots for (c) 2153 and (d) 2203 UT. Increment at contour lines is 0.4 $\mu A/m^2$.

Correspondingly, a second negative center is formed in the evening sector at around 2000 MLT and is intensified at around 2202 UT to take over the dominance of the afternoon cell from the previous center located at around 1500 MLT. To qualify the remarks of stepwise rather than continuous changes it is important to stress, that the database for these AMIE plots includes the magnetic data from the Greenland stations listed in Table 1. At the time of the event these stations are located in the evening quadrant and provide a good coverage of the region where the most dynamic changes took place.

In order to further quantify the changes in convection structure Figure 4a and 4b display enlarged versions of the AMIE potential patterns at 2153 and 2203 UT, respectively. In these plots the position of STF has also been marked by a dot like in Figure 3. At 2153 UT, STF is located well within the rather uniform transpolar plasma flow. At 2203 UT the station is located poleward of, but close to the center of the afternoon convection cell. In the potential plot for 2153 UT (Figure 4a) STF is located at the +21 kV contour curve while at 2203 UT (Figure 4b) it is located at the -39 kV potential contour. Hence, during the 10 minutes separating the two potential plots the potential at STF has changed by a total of 60 kV (these values are highly approximate). Another set of relevant observations concerns the horizontal (ionospheric) electric field strengths in the vicinity of STF. At 2153 UT the electric field around STF is rather uniform at around 60 mV/m in the westward direction. At 2203 UT, in contrast, STF is close to the field reversal. Poleward of STF the field strength is around 50 mV/m in a direction a little west of south. Equatorward of the field reversal the field strength is also around 50 mV/m, while the direction in this region is due northward.

Figures 4c and 4d present the corresponding polar maps of field-aligned current intensities derived from the AMIE calculations at 2153 and 2203 UT, respectively. The solid lines represent contours of downgoing field-aligned currents while the dashed contour lines represent upgoing currents. The contours mark increments of 0.4 $\mu A/m^2$ in the field-aligned current intensities. The main development from Figure 4c to 4d is the appearance at 2203 UT of a region of upward field-aligned currents at latitudes of around 72° and magnetic local times

around 1900 MLT. The diagram in Figure 4d represents the maximum phase of this current system. The peak intensity (in AMIE resolution) is around 2 $\mu A/m^2$.

These observations will be referenced below. One should note, however, that the numerical values have been derived from the smoothed and interpolated output from the AMIE procedure. Hence they represent, at best, large-scale spatial and temporal averages of the highly variable, real quantities. Furthermore, the AMIE potential plots like those in Figures 3 and 4a-4d can only represent the spatial and temporal details of the convection structure that are derivable from the geomagnetic observations. These observations, having typically 20-s to 1-min temporal resolutions, and with inherent, nonresolved sensitivity to ionospheric current systems within a few hundred km, can hardly provide much further reliable resolution in the AMIE output than ~1 min and ~200 km, respectively.

The imaging riometers (IRIS), however, can provide further resolution of the spatial and temporal details of the processes. The radio wave absorption features detectable by riometers correspond to ionization enhancements in the ionospheric *D* and *E* regions at approximately 70-120 km of altitude. These features are also part of the substorm event. Such ionization enhancements are usually caused by precipitation into the atmosphere of high-energy charged particles, typically electrons in the 10-100 keV energy range. Temperature enhancements related to the electron heating in strong electric fields may in some events cause (usually weak) absorption enhancements [*Stauning*, 1984]. The available IRIS instruments provide "images" of the ionospheric absorption of radio waves by measuring the varying intensities of cosmic noise signals received within each of an array of beams in different directions. The measured intensities are then compared to the undisturbed "quiet day" (QD) levels to derive the ionospheric attenuation of the signals. The temporal and spatial resolutions for the absorption images are 1 s and ~20 km, respectively. During substorm events the peak absorption intensities are typically ~2-3 dB (at 38 MHz).

Figure 5 presents the imaging riometer observations from STF along with the magnetometer and normal-beam riometer measurements for the time interval 2000-2400 UT on November 4, 1993, corresponding to Figure 2. All displayed data are 1-min averages. Figures 5a-5c display the 38-MHz cosmic noise signal levels recorded in beams selected to represent the entire field-of-view of the imaging riometer system. The signal levels have been normalized such that the undisturbed signal would give horizontal lines in the plots. Absorption (reduction in signal level) is positive downward. Figure 5a displays data from the second-northernmost row of beams arranged in sequence from west (upper beam) to east (lower beam). Figure 5b presents the signal levels for the central row of beams again in sequence from west to east. The middle beam in Figure 5b is directed toward zenith. Figure 5c displays the signals from the second-southernmost row of beams. Figure 5d displays magnetometer and normal-beam riometer data. The three upper traces in this panel depict the *H*, *E*, and *Z* components. The three lower traces display the wide-beam 24-, 30-, and 31-MHz riometer signal levels for reference to similar observations [e.g., *Imhof et al.*, 1984]. Figure 5 displays an interval of almost 2 hours of quiet conditions at STF. At 2143 UT the poleward expanding substorm phase, which was first seen in NAQ at 2130 UT, reaches the southernmost beams of the imaging riometer in STF starting a disturbed period lasting for around 20-25 min.

Further details of the combined temporal and spatial substorm development are provided in the diagrams in Plate 1, which present color-coded cosmic noise absorption intensity images derived from the IRIS observations at STF. The absorption intensities are defined by the scale at the top of the diagrams. The orientation and the dimensions of the images are illustrated in the last frame in the bottom row. Each small frame presents an absorption image of dimensions 240×240 km (using a reference height of 90 km) centred over STF. Geomagnetic north is upward in the diagrams. Plate 1a spans the time interval from 2136 to 2217 UT. The data plotted in this diagram are 1-min average values. There is 1-min separation from frame to frame in the sequence.

It is seen, that an absorption event arrives at the southern edge of the field of view at about 2143 UT. During the next 5 min the event expands poleward across the field of view at a speed of about 1 km/s. At 2150 UT the event appears to stagnate and then, during the next 5 min, it retreats equatorward while fading. At 2156 a WNW-ESE oriented arc-like structure appears just poleward of Sdr. Strømfjord. This structure moves slowly equatorward while rotating to NW-SE orientation. At 2201 UT the event suddenly intensifies very strongly to reach peak intensity in the image at 2203 UT. A fast equatorward motion of the intensity peak is seen during the maximum phase. Then, at 2205 UT the event fades away. Plate 1b presents the maximum phase of the absorption event on a more detailed timescale. The data are 10-s averages, and there is also 10 s between frames. It is seen here that the peak phase comprises three separate enhancements maximizing at 2201:25, 2203:05, and 2203:35 UT respectively. One may also note how the orientation of the region of high absorption changes from being nearly E-W directed during the approach of the poleward expanding event seen first at 2143 UT to being NW-SE directed at the start of the major enhancement at 2201 UT. At the end of this phase, in the frames for 2203:50 UT and 2204:00 UT, the absorption structure is almost N-S oriented.

It is seen from the display in Plate 1b that the absorption is particularly intense in a band stretching from SE to NW. The centerline of the band is a little equatorward of the central diagonal of the antenna field. In the beams around and just equatorward of the SE-NW diagonal the absorption intensities fluctuate around 4-8 dB during the event to reach maximum intensities of around 14 dB for a few of the central beams within the 2203 UT minute. The absorption intensities in the northeastern beams and in the southwesternmost beam reach 2 dB only.

To derive the dimensions of the structure, it should be noted that the absorption processes must extend over the entire width of the beams involved during the more intense events. In case they were limited in width to a narrow strip compared to the IRIS beamwidth (≈20-30 km) then the absorption intensities would reach at most the geometrical ratio of the disturbed to the undisturbed projected beam area. The width of the intense absorption region is generally 50-100 km. For the individual high-intensity peaks the widths are estimated to 30-40 km. The longitudinal extent of the absorption region is greater than the length (~340 km) of the diagonal of the beam projection. Most of the observed decreases in absorption intensities in the northwesternmost or southeasternmost beams are compatible with the widening of the projected beam area for the more oblique beams related to the estimated width of the absorption region.

A further diagram to disclose the temporal structure of the

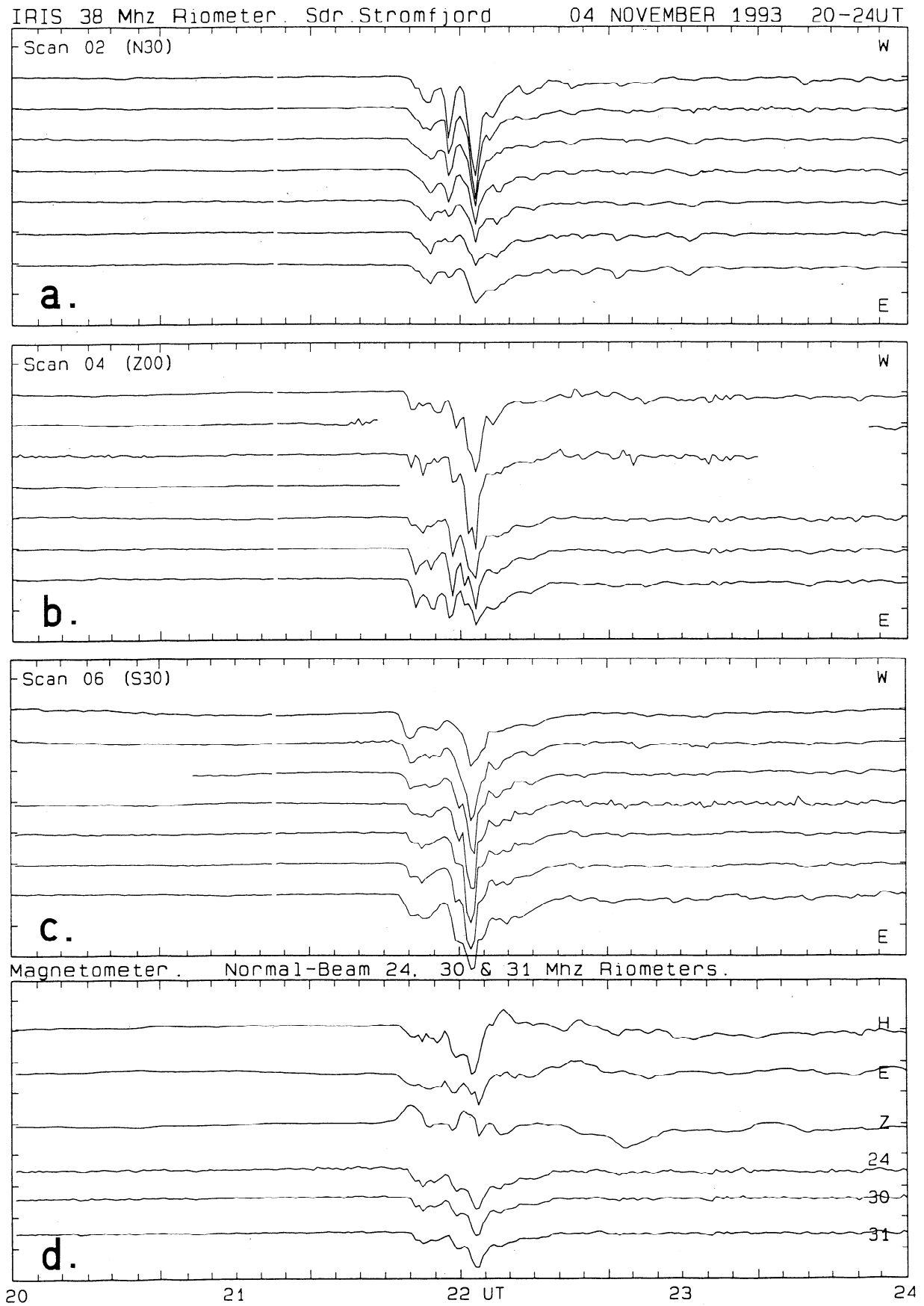

Figure 5. Imaging riometer (top three panels), magnetometer and normal-beam riometer observations from Sdr. Strømfjord during 1800-2400 UT on November 4, 1993. Absorption is positive at downward deflections in the riometer traces.

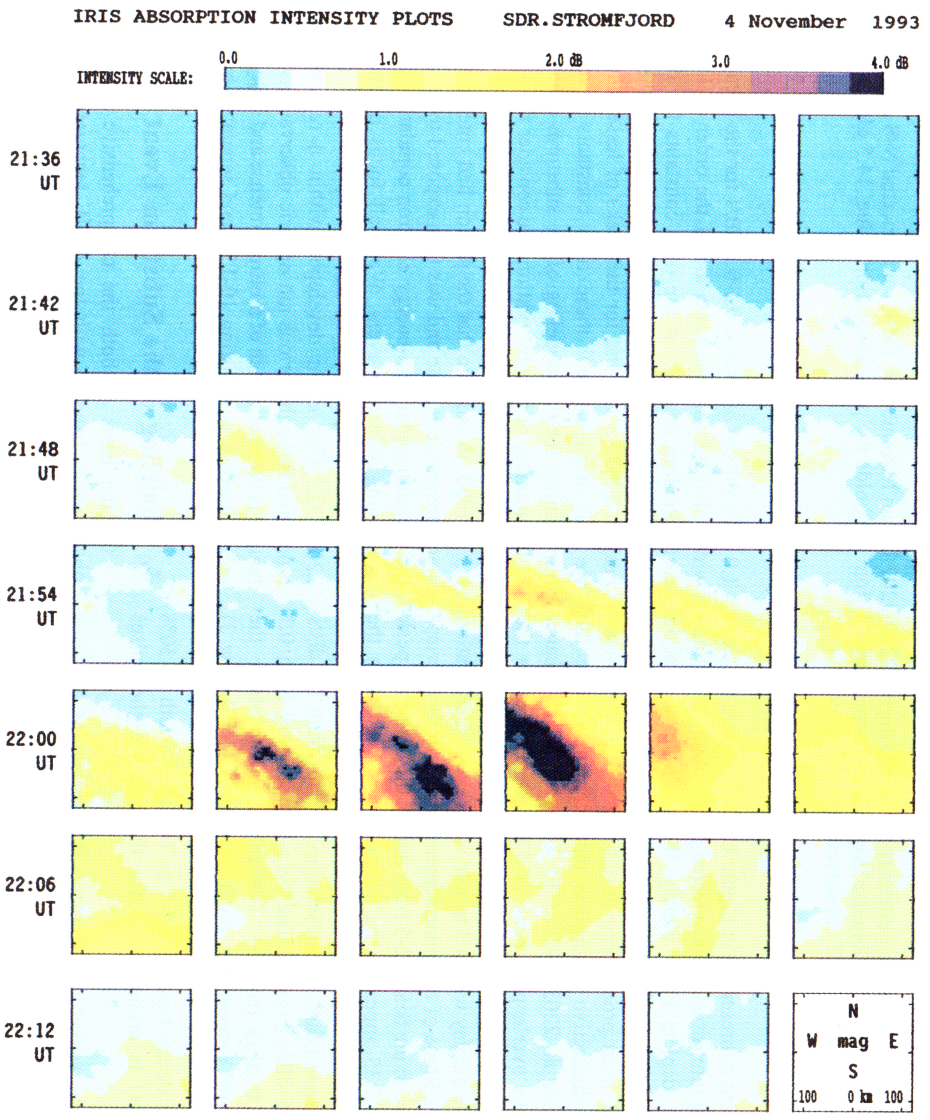

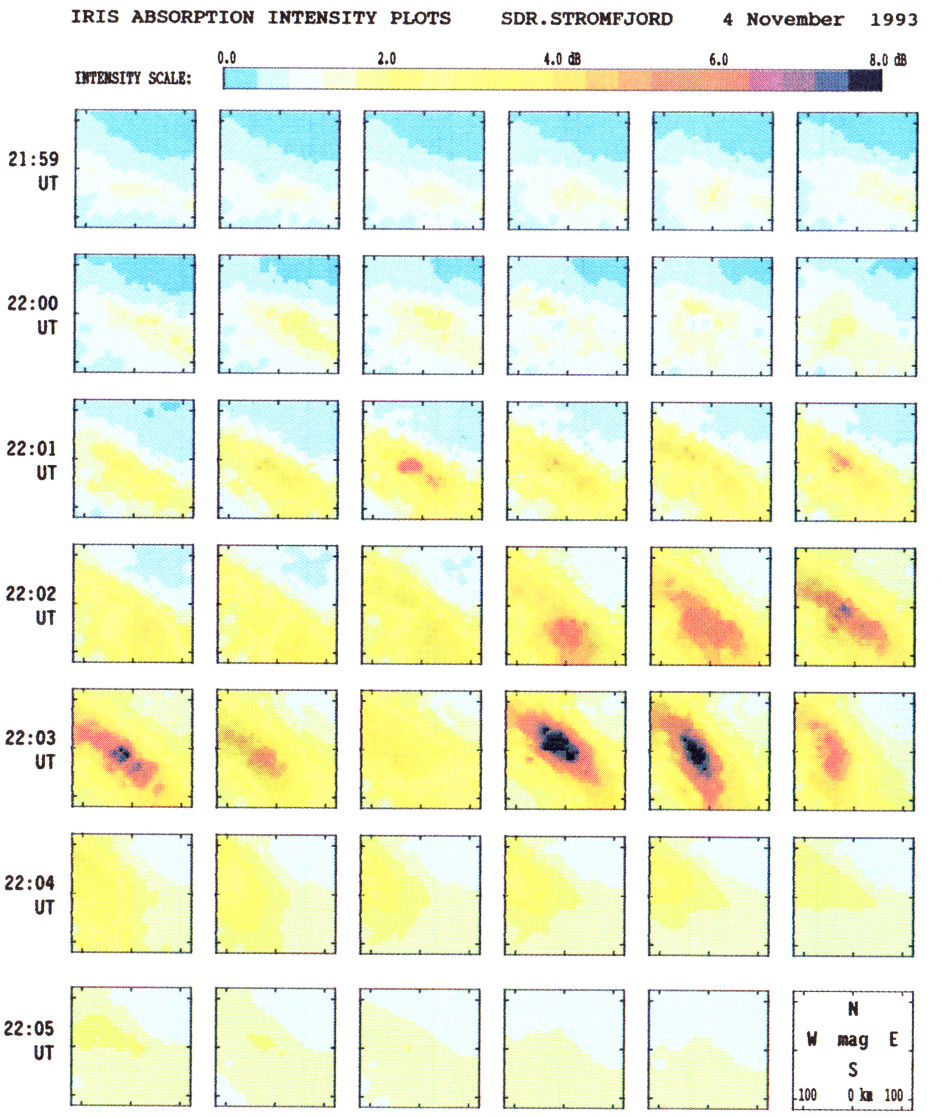

Plate 1. IRIS imaging riometer absorption intensity images for the early evening substorm at ~2200 UT on November 4, 1993, observed in Sdr. Strømfjord: (a) 1-min average values 2136-2216 UT and (b) 10-s average values 2159-2206 UT.

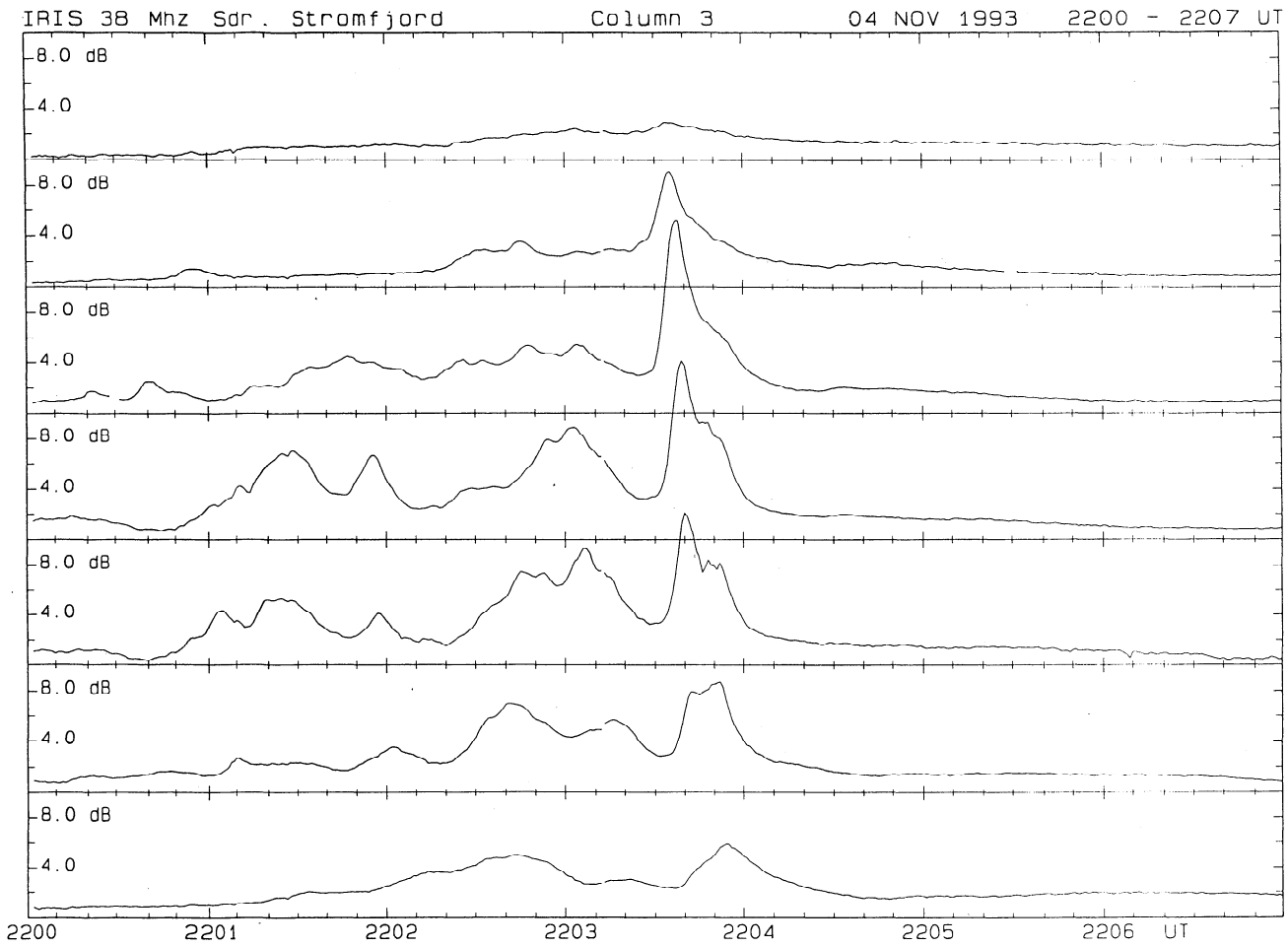

Figure 6. Absorption intensity variations during 2200-2207 UT on November 4, 1993, for a selected N-S column (no. 3) of imaging riometer beams. The beam in row 3 from top holds the peak absorption value, 14.5 dB (at 38 MHz) at 2203.35 UT, observed during the event.

absorption event is presented in Figure 6. The diagram presents 1-s absorption intensities for a selected N-S column of beams. This diagram depicts more clearly the multiple absorption enhancements and their risetime and decay time. The first starts at 2200:50 UT most pronounced in row 3 and 4. Then follows at least four distinctive absorption enhancements before the prominent peak at 2203:30-2203:40 UT seen in all beams followed by an overlapping peak at 2203:50 UT seen in the southern beams only. The seven major separate enhancements observed in the display within 3 min have an average separation of around 26 s. Some of the enhancements are partially overlapping. However, in the beams 2-5 from the top the dominant peak at around 2203:35 appear to be adequately isolated from the other enhancements such that onset and decay slopes are well defined. For these beams the onset slopes varies from 1.0 dB/s (row 2) to 2.5 dB/s (row 3). The decay slopes vary from 0.7 (row 2) to 2.0 dB/s (row 3). The enhancements above the estimated "level" ranges from 6 dB (row 2) to 11 dB (row 3) such that the 10% to 90% pulse risetime is 4-5 s while the corresponding decay times are 5-7 s. The total width at 50% amplitude level is around 12 s for the most of the pulses observed.

For the other, weaker enhancements the overlapping of pulses prevents a correspondingly detailed analysis of onset and decay slopes. The values inferred from the display are around 0.5 to 1.0 dB/s for the onset and 0.3-0.5 dB/s for the decay. The 50% width of these enhancements are of the order of 15-30 s. The corresponding analysis of the time constants for the different columns of beams give similar results both for the prominent peak at 2203:35 UT and for the peaks of lesser amplitude. As we will discuss below these time constants have important implications for the modeling of the substorm events.

In summary of the observations we consider the weak absorption disturbances passing over STF at 2143-2150 UT on November 4, 1993, to indicate that the station had entered the "closed" magnetospheric regime and was then exposed to precipitation of the pseudotrapped high-energy electron population arising from a decaying substorm event. We shall focus on the relatively simple and exceptionally strong substorm that occurred at 2156-2206 UT. This event developed within a region very well monitored through various ionospheric observations. A specific feature is the occurrence of multiple intense and spiky absorption enhancements each lasting 10-15 s and separated by 20-30 s.

4. Modeling of the Substorm Event

On the basis of both the comprehensive polar magnetic observations handled with the AMIE technique and the local observations from STF of the disturbance events observed at around 2200 UT on November 4, 1993, we shall attempt a

modeling of the processes involved. This event appears particularly well suited for modelling efforts since it was preceded by an extended interval of rather quiet conditions and thus well isolated from other events. The general polar potential patterns preceding and following the event were simple. The event was very intense; thus the signatures in the various observations are exceptionally strongly marked.

The modelling of substorm events has three elements, namely, (1) the large-scale magnetospheric processes leading to substorm disturbances in general, (2) the processes occurring along the field lines connecting the ionosphere to the magnetosphere, and (3) the ionospheric processes controlling, among others, the ionospheric conductivities and the radio wave absorption intensities. In this paper we shall briefly touch upon the general magnetospheric conditions and then concentrate on the latter two subjects.

The changeable polar ionospheric convection patterns are mainly controlled by the magnetospheric plasma convection processes powered by the solar wind conditions and also affected by substorm-related reconfiguration processes in the outer magnetosphere and tail regions. The ionospheric processes have feedback effects (like drag or loading) on the magnetospheric convection conditions. Hence the electrodynamical properties of the field line connection are extremely important for the properties of the coupled solar wind-magnetosphere-ionosphere system.

The upper ionospheric/magnetospheric plasma environment holds three components: (1) a "cold" ionospheric plasma with densities up to 10^6 electrons/cm^3 and typical temperatures of 3000 °K ($E_e \approx 0.25$ eV), (2) a "hot" magnetospheric plasma with densities of around 0.5 to a few electrons/cm^3 and temperatures corresponding to 0.2-2.0 keV, and (3) a high-energy charged particle population with densities less than 0.1 cm^{-3} of electrons and protons of energies up to a few hundred keV. The two first components are assumed to have Maxwellian distributions. The assumed characteristics of the population of high-energy particles used in the modelling below are based on typical satellite results.

The suggested model to explain the reported high latitude, early evening substorm event assumes that the intense upward field-aligned currents required to modify the ionospheric convection pattern following a reconfiguration of magnetospheric flow patterns can create large potential drops along the connecting field lines. Such potential structures will accelerate and precipitate magnetospheric electrons which, in turn, will enhance the ionospheric conductivities. The conductivity enhancements will cause reduced horizontal electric fields or increased currents which may provide positive feedback effects to the field-aligned potential drops. Such feedback effects to accelerate the processes was suggested, for instance, by *Ogawa and Sato* [1971], *Rothwell et al.* [1984], *Kan et al.* [1984, 1988], and *Lysak* [1986]. The new features added here from the reported observations are the impulsive character of the processes and the multiplicity of events. Each individual case of enhanced field-aligned potentials seems to have a short duration of a few seconds only. Series of such events may gradually energize magnetospheric plasma electrons and contribute to the high-energy electron population observed in the auroral zone and the radiation belts further inside the magnetosphere.

4.1. Magnetospheric Processes

According to the Geotail satellite observations at ~200 R_E [see *Knipp et al.*, this issue] the solar wind conditions in the evening of November 4 were characterized by a high-velocity, low-density plasma flow. The interplanetary magnetic field (IMF) was weak with all components fluctuating around zero. There are, however, no definite observations of the conditions at the time in question (~2200 UT) since Geotail was moving in and out of the flapping magnetotail. At 2200 UT on November 4 the IMP 8 satellite at a position of $(X_{GSM}, Y_{GSM}, Z_{GSM}) \approx (-35, 12, 11\ R_E)$ was in the magnetospheric tail region. In the IMP 8 magnetometer data [see *Knipp et al.*, this issue] the B_Z (GSM) component of the magnetic field was consistently negative at -2 to -4 nT during the hour preceding the selected event. The B_Y component was small while the B_X component was positive and large, but decreasing. The negative value of B_Z indicates a large deformation of the tail field since the undisturbed geomagnetic field would have a positive Z component. There are no dramatic field changes seen at the time corresponding to the substorm onset.

The present study deals primarily with the conditions during the selected event at ~2200 UT in the regions magnetically connected to the location of STF (invariant latitude=73.7°) in the magnetic local time sector at around 2000 MLT. Earlier in the evening, up to around 2140 UT, STF appears connected to the "open" magnetospheric tail lobe region void of high-energy electrons which could cause absorption. The continued substorm activity at lower latitudes since 2130 UT (see Figure 2) has apparently changed the configuration in the tail region such that the ionospheric projection of the boundary between the "open" and "closed" magnetospheric regions was moving to a position poleward of STF at 2153 UT. The distinguishing between "open" and "closed" magnetospheric regions assumes that high-energy particle radiation, like that responsible for the absorption event seen in STF during the event, is constrained to the "closed" magnetospheric regime.

The development of the convection patterns seen in the AMIE potential plots during the 10 min from 2153 to 2203 UT, as displayed in Figures 3 or 4a and 4b, indicates that the relative location of STF shifts from a position well within the transpolar flow to a position at or a little poleward of the evening ionospheric convection reversal boundary. This boundary maps to magnetospheric flow reversal regions where the plasma flow changes from antisunward to sunward flow direction. Such shear regions are considered to be generator regions for the field-aligned currents that connect to the ionospheric convection reversal regions, but the exact nature of the generator mechanisms has not yet been fully resolved [see, e.g., *Vasyliunas*, 1979; *Sonnerup*, 1979; *Lundin and Evans*, 1985; *Lotko et al.*, 1987; *Siscoe et al.*, 1991; *Lundin et al.*, 1991].

We interpret the sudden shift in the ionospheric convection patterns relative to the position of STF to be the consequence of a major magnetospheric reconfiguration in the tail region which is subsequently conveyed to the ionosphere through strong field-aligned currents.

4.2. Field Line Processes

An important element of substorm studies is the possible build-up of large potential differences along the geomagnetic field lines. The current-voltage relationship along auroral field lines have been discussed theoretically by, among others, *Knight* [1973], *Lemaire and Scherer* [1974, 1978]; *Fridman and Lemaire* [1980], *Lyons* [1980, 1992], *Lu et al.* [1991], *Borovsky* [1993], and *Pierrard* [1996]. On the basis of observations the current-voltage characteristics of auroral field lines have been examined by *Lyons et al.* [1979], *Weimer et al.* [1985, 1987], and *Brüning et al.* [1990]. For a location close to the evening

convection reversal the dominant type of field-aligned currents is the large-scale upward region 1 currents [*Iijima and Potemra*, 1976, 1978]. These currents involve the downward flow of magnetospheric electrons against a converging geomagnetic field. Their magnitudes have been estimated from satellite-based magnetometer observations to be of the order of one or a few $\mu A/m^2$ (reduced to ionospheric altitudes) during moderately disturbed conditions. During very disturbed conditions upward field-aligned currents of up to several tens of $\mu A/m^2$ have been observed [e.g., *Brüning et al.*, 1990].

The plasma environment along the field lines that connect from the magnetospheric flow shear regions to the ionospheric convection reversal regions, located close to STF during the peak of the event considered here, is characterized by the three above mentioned plasma component. From the top of the ionosphere, at altitudes of a few hundreds of kilometers, the density of the cold ionospheric plasma component decreases strongly. From altitudes of one or a few R_E and further out the high-temperature, low-density magnetospheric plasma becomes dominant. Plasma densities of around N=1 cm^{-3} and temperatures of a few hundred eV to a few keV are considered typical for the high latitude outer magnetosphere [e.g., *Lyons*, 1992].

For ionospheric altitudes the electron densities, and hence the conductivities, are so high that the potential drops required to drive field-aligned currents of the above intensities will be small. For the low-density plasma environment in the outer magnetosphere a substantial potential drop may be required to drive such currents in the converging geomagnetic field. For a Maxwellian electron distribution with isotropic pitch angle distribution the parallel current density referred to ionospheric heights can be written [e.g., *Lyons*, 1992]:

$$J_\parallel = eN_o\left(\frac{K_{th}}{2\pi m_e}\right)^{1/2} R\left\{1-(1-R^{-1})\exp\left(\frac{-e\Phi_\parallel}{K_{th}(R-1)}\right)\right\} \qquad (1)$$

where $J_\parallel$ is the upward parallel current carried by the magnetospheric electrons. $\Phi_\parallel$ is the potential difference between the ionosphere and the top of the field-aligned potential variation, while K_{th} is the thermal electron energy. $R=B_i/B_m$ is the ratio between the magnetic field B_i in the ionosphere and the magnetospheric field B_m. For intermediate values of $\Phi_\parallel$ such that $1 \ll e\Phi_\parallel/K_{th} \ll R$ equation (1) approximates a linear "Ohm's law":

$$J_\parallel \approx K\Phi_\parallel \qquad (2)$$

where $K=e^2N_o/(2\pi m_e K_{th})^{1/2}$ is the parallel "conductance," e and m_e being the electron charge and mass while N_o is the magnetospheric electron density. The potentials $\Phi_\parallel$ required according to (2) to drive upward currents of 1-10 $\mu A/m^{-2}$ are $\Phi_\parallel$~1-10 kV for typical values of N_o=1 cm^{-3} and K_{th}=0.5 keV. Such field-aligned accelerating potentials of the order of 1-10 kV have been deduced for the high-latitude evening regions from observations of precipitated electrons [e.g., *Evans*, 1974], from the occurrence of upward ion beams [e.g., *Gorney et al.*, 1981], and from direct observations of the electric fields in space [e.g., *Brüning et al.*, 1990].

Furthermore, equation (1) indicates that the parallel currents (transformed to ionospheric level) may saturate and asymptotically approach the value

$$J_\parallel(\max)=eN_o\left(\frac{K_{th}}{2\pi m_e}\right)^{1/2} R \qquad (3)$$

as the value of $e\Phi_\parallel/K_{th}$ increases indefinitely. It is seen that the limiting value decreases with decreasing altitude (decreasing R). However, it should be noted that (1) to (3) assume constant plasma density and temperature along the field line and, consequently, will fail as one approaches the ionosphere where the ionospheric electrons add to the magnetospheric electron population. Consequently, the current limiting and hence the assumed formation of large accelerating potentials will occur at some intermediate altitude between the ionosphere and the equatorial magnetosphere.

Satellite observations have indicated that for the evening auroral regions the potential drops are particularly large at intermediate heights of 1-2 R_E [*Lin and Hoffman*, 1979; *Gorney et al.*, 1981; *Brüning et al.*, 1990]. A similar result was derived by *Lemaire and Scherer* [1978] from model calculations of the electric potential distribution along mantle field lines. At these altitudes, R will have a value of $R\approx 20$. Here the contributions from magnetospheric electrons given by (1) dominate the field-aligned current intensities. For the above plasma parameters the asymptotic value of the field-aligned current intensity derived from (3) is 12 $\mu A/m^2$. Such high values are occasionally observed from satellites [*Brüning et al.*, 1990].

A possible sequence of processes could be the following: The divergence of the horizontal ionospheric currents increases locally. The resulting parallel current may approach the limiting intensity defined by (3) at some intermediate altitude level resulting in the formation of large field-aligned potential drops (inverted-V structures). The electrons exposed to this potential drop will be accelerated toward the ionosphere. Those not mirrored by the converging magnetic field will be precipitated into the dense atmosphere at ionospheric altitudes (~100 km) whereby its conductivity is increased. The increase in ionospheric conductivities, notably the Pedersen conductivities will either for a given (saturating) current decrease the ionospheric fraction of the total potential available and hence increase the field-aligned potential drop or for a given potential distribution further increase the currents drawn from the magnetosphere giving a positive feed-back effect in both cases. The accelerated primary electrons, in addition, will generate an upward flux of secondary and backscattered electrons [e.g., *Banks et al.*, 1974] which will approach (and be reflected by) the above potential structure. The potential structure will move upward as a consequence of the addition of secondary and backscattered electrons from below. Furthermore, electrons from ambient flux tubes will diffuse toward the depleted region causing the potential drop. These effects will tend to reduce the accelerating potential and move it further away from the ionosphere with the result that the energetic precipitation decreases. Now the ionospheric conductivities are reduced. The ionospheric currents will now decrease, the horizontal potential drop will increase, and the feedback effect will quench the field-aligned potential drop as fast as it was generated.

The combined result of these processes is the sudden formation of a large potential drop over a fraction of the field line at some intermediate altitude. The potential structure will grow to maximum amplitude and then rapidly decay. During the growth phase the structure will develop an upper region of (primary) electron depletion and a lower region of excess (secondary and backscattered) electrons. The time-varying structure is related to ionospheric changes the effects of which, most likely, are conveyed from the ionosphere to the magnetospheric acceleration region in the form of kinetic (oblique) Alfvén waves with velocities as defined through the dispersion relation [e.g., *Goertz*, 1984]:

$$\omega = k_{\parallel} V_A (1 + k_{\perp}^2 c^2/\omega_{pe}^2)^{-1/2} \quad (4)$$

where $V_A = B/(\mu_o(m_e+m_i)N_o)^{1/2}$ is the Alfvén velocity. The waves will be damped as the nonequilibrium electron distributions are leveled out by drift and diffusion. In the limit of weak ionospheric feedback effects the evanescent wave may give a stable inverted-V structure. However, in the other limit of strong feedback effects, as one would expect during active substorm conditions, the result is rather the sudden formation at intermediate altitudes of large acceleration potential structures which then rapidly fade away.

The Alfvén velocity V_A determines the order of magnitude of the timing involved. At ionospheric altitudes, where $B \approx 50{,}000$ nT, and $N_o \approx 10^6$ cm^{-3}, we have $V_A \approx 1000$ km/s. At the above assumed altitude of around 2 R_E the magnetic field has decreased to $B \approx 2500$ nT and $N_o \approx 1$ cm^{-3}, we find $V_A \approx 50{,}000$ km/s. Since the speed of propagation along the field direction of a kinetic Alfvén wave is a fraction of the order of unity of V_A and since the feedback process involves communication between the ionosphere and the acceleration region then we see, that the risetime and decay time for the field-aligned potential structures will be of the order of a few to a few tens of seconds.

These times are of the same order of magnitude as the bounce period at the latitude in question for the accelerated electrons with energies from a few to a few tens of keV [*Roederer*, 1970]. The similarity in time constants for the potential variations and the electron bouncing opens the possibility for enhanced effects arising from multiple triggering of impulsive potential structures by bouncing electron clouds that are, in turn, further intensified by being exposed repeatedly to the positive phase of the accelerating potentials. The maximum energy increment that the electrons may receive without being precipitated is obtained by those electrons of the population that were initially mirroring at the altitude of the acceleration potential structure. Their energy increment can be $R=B_i/B_a$ times the initial energy E_o. If $R \approx 10$-30 and $E_o \approx 1$-10 keV (for the upper part of the distribution) then we see that the energy increment can amount to several tens or a few hundreds of keV. Field-aligned potential drops correspondingly large are not feasible, but the energization could also be obtained by repeated acceleration in time-varying electric fields. Each enhancement will cause precipitation and associated conductivity changes which can make the feedback effect work. In the end a fraction of the initial electron population can be accelerated to very high energies. One may note that the power of this mechanism in terms of energy increment will increase with increasing R. Thus it is important to consider the possibility that the potential structure can move out along the field line in a wave-like manner.

4.3. Ionospheric Processes

The polar ionospheric plasma convection for which the AMIE potential contours provide the approximate flow patterns is an important element of the substorm model. For the substorm at around 2200 UT on November 4, 1993, the convection displayed a major shift between two relatively simple two-cell convection patterns. For STF the shift had at least two essential consequences: (1) the location of STF relative to the general magnetospheric configuration shifted from being in the magnetically "open" polar cap prior to the event to being during the event in the "closed" magnetospheric region very near the afternoon convection reversal boundary. (2) Before the event the ionospheric electric field and current systems at STF were characterized by being part of a rather homogeneous transpolar convection system with moderate horizontal electric fields and currents and small field-aligned current intensities. At the peak of the event the local ionospheric potential had shifted level by 50-60 kV in less than 10 minutes and the local convection pattern had markedly shifted shape and direction. To accomplish such large changes requires strong field-aligned currents to couple between the magnetospheric and the ionospheric reconfigurations.

To reach an initial order of magnitude estimate of the intensities of the field-aligned currents involved, we may consider the potential patterns displayed in Figure 4b. The geometry indicates that the field-aligned currents are 2-3 times more intense at the tip of the "nose" of the potential contours than further back. The magnitude of the horizontal electric fields in the region around the convection reversal are of the order of 50 mV/m. The height-integrated Pedersen conductivity in this region is around 4 Ω^{-1} during weakly disturbed conditions [*Ahn et al.*, 1983]. Assuming further that the field-aligned currents are flowing within the region of active absorption disturbances as depicted by the STF imaging riometer observations, we may derive a width of the current sheet of 50-100 km. Hence the field-aligned current intensities are 2-4 μA/m^2 for the flow reversal region averaged over the width of the current sheet and possibly 2-3 times larger at the tip of the flow reversal region. These coarsely estimated values, which are larger than those estimated from the AMIE plots in Figures 4d but still averages through the main phase of the substorm, will need field-aligned potentials of some kV in order to be supported by typical magnetospheric plasma structures. Hence we could expect that large potential differences will be generated along the geomagnetic field lines connecting from the ionospheric convection reversal region to the magnetospheric region. An indication of the large potentials involved is the change in ionospheric potential by 50-60 kV overhead STF during the 10-min transition from presubstorm to peak substorm conditions. On these conditions it seems quite realistic that a model for the present very intense substorm case will comprise field-aligned currents of peak values up to 10-30 μA/m^2 driven by impulsive field-aligned potentials of 10 to 30 kV.

We are now in a position to attempt a modelling of the ionospheric disturbances resulting from precipitated flux of accelerated energetic electrons. Following *Evans* [1974] we assume the presence of an accelerating potential V_o which occurs at some altitude above the ionosphere. If the initial electron distribution is isotropic then the flux of the accelerated electrons at the bottom of the acceleration region is also isotropic within a pitch angle cone of half angle $\alpha_o = \sin^{-1}[E/(E+e\,V_o)]^{1/2}$. The directional flux within this cone can be written [*Evans*, 1974]:

$$j(E+e\,V_o,\alpha) = N_o \frac{E+e\,V_o}{(2m_e\pi^3 E_o^3)^{1/2}} \exp(-E/E_o) \quad (5)$$

where E is the primary electron energy, N_o and E_o are the magnetospheric electron density and characteristic energy, while m_e and e are the electron mass and charge. The total flux of electrons at energy $E+e\,V_o$ that actually reaches the ionosphere can then be derived by integration of the flux over pitch angles from zero to the smaller of α_o and α_a where the latter is the pitch angle at the acceleration altitude for electrons that mirror at ionospheric altitude. Hence $\alpha_a = \sin^{-1}(B_a/B_i)^{1/2}$, where B_a and B_i are the magnetic fields at acceleration altitude and at the ionosphere.

The ionization rate s_{jk} at height h_j for a monoenergetic beam of electrons with energy E_k and unit downward flux is calculated

from

$$s_{jk} \equiv s(h_j, E_k) = \frac{E_k\, L(Z(h_j)/R_k)\, M'(h_j)}{\Delta E_{ion}\, M'(d_k)\, r_k} \quad (6)$$

where $L(Z(h_j)/R_k)$ is the normalized distribution function for the energy losses for energetic electrons entering the atmosphere [*Rees*, 1963, 1969]. This function depends on the atmospheric depth $Z(h_j)$ at altitude h_j over R_k, the atmospheric depth at d_k which is the altitude of maximum penetration for an electron of energy E_k. $M'(h_j)$ is the effective number density (corrected for composition) of neutrals at height h_j, while $M'(d_k)$ is the corresponding number density at d_k. The normalized penetration depth is $r_k=R_k/\rho_k$ where ρ_k is the mass density at altitude d_k. ΔE_{ion} is the average ionization energy (≈35 eV).

With a known energy spectrum for the particle flux $f_k=f(E_k)$ the total ionization rate at height h_j can be derived by integration over all primary energies, hence

$$Q_j^* \equiv Q^*(h_j) = \int_k s_{jk} f_k \, dE_k \quad (7)$$

From the ionization rate Q_j^* due to precipitation of energetic magnetospheric particles and the corresponding ionization rates, Q_j^{EUV} due to solar EUV radiation and a small contribution Q_j^{**} from other sources (e.g., cosmic radiation), one may derive the time-varying electron densities N_j at height h_j from the continuity equation:

$$dN_j/dt = Q_j^* + Q_j^{EUV} + Q_j^{**} - K_j - N_j \nabla \cdot \boldsymbol{v}_j - \boldsymbol{v}_j \cdot \nabla N_j \quad (8)$$

where K_j is the recombination rate and $\boldsymbol{v}_j$ the ionization drift velocity at h_j.

For the event in question the ionosphere is in darkness for the heights of interest. Hence the Q_j^{EUV} term can be neglected. Q_j^{**} holds the residual ionization sources which are of some importance in the lower D region. The last two terms in (8), which define the contributions from drift of ionization, are important in the upper ionosphere (F region) but are usually small in the lower ionospheric regions (D and E regions) which are considered here. The recombination rate K_j is a complicated function of ion chemistry and electron density. In the numerical calculations it has been expressed in terms of a variable effective recombination coefficient defined through

$$K_j = \alpha_{eff} N_j^2 \quad (9)$$

With N_j^o being the residual electron density that would be present without incident energetic magnetospheric electron precipitation then (8) transforms into the simpler (approximate) expression:

$$dN_j/dt = Q_j^* - \alpha_{eff}(N_j - N_j^o)^2 \quad (10)$$

where it is assumed that the inclusion of N_j^o takes into account the small residual terms in (8). Now in steady state, where $dN_j/dt=0$, we have

$$N_j = N_j^o + (Q_j^*/\alpha_{eff})^{1/2} \quad (11)$$

The residual electron density values are here derived from the series of empirical electron density profiles for 60-130 km altitude versus solar zenith angle and riometer absorption intensities given by *Friedrich and Torkar* [1983] using zero absorption intensity and their table of coefficients for the night profiles. The table is based mainly on measurements of the electron density profiles by rocket instruments launched from Andoya in North Norway located at a geographical latitude close to that of STF. The condition of zero absorption is assumed to correspond to cases with no energetic electron precipitation.

Following the procedures and programs developed by *Kirkwood* [1988] and *Kirkwood and Osepian* [1996], the recombination rates in the upper E region, at altitudes h_j>110 km, are described by using a fixed value of the recombination coefficient in (9):

$$\alpha_{eff}(h_j>110 \text{ km}) = \text{const} = 2\times10^{-7} \text{ cm}^3 \text{ s}^{-1} \quad (12)$$

whereas for the lower E region and the D region, at h_j<110 km, a simplified ion-chemistry model is used in the calculations of $\alpha_{eff}=\alpha_{eff}(h_j)$. The model developed by *Torkar and Friedrich* [1983], *Velinov et al.* [1984], and *Smirnova et al.* [1988] considers positive and negative ions of the major constituents (N_2, O_2, N, O) and of selected minor constituents (H_2O, CO_2, Cl_2, NO, O_3, and $O_2(^1\Delta_g)$). A reaction scheme for the formation of positive and negative ions is presented in Figure 2 of *Kirkwood and Osepian* [1996] and the reaction rates are defined in their Table 1. The model profiles for the concentrations of the minor constituents are defined in their Table 2. The concentrations of the major constituents and the neutral atmospheric temperatures are calculated from the MSIS-90 model (a further development of the MSIS-86 model [*Hedin*, 1987, 1991]) using as input parameters to the program the geographic coordinates for STF, the actual values for the time and date of the event, the relevant solar 10.7-cm flux, and geomagnetic activity parameters.

The height-dependent Pedersen and Hall conductivities $\sigma_{H,j}$ and $\sigma_{P,j}$ have been derived from standard formulas [e.g., *Brekke and Moen*, 1993]:

$$\sigma_{P,j} = \frac{N_j e}{B_j} \left\{ \frac{\omega_{ce}\nu_{en}}{\omega_{ce}^2+\nu_{en}^2} + \Sigma_m P_m \frac{\omega_{ci,m}\nu_{in,m}}{\omega_{ci,m}^2+\nu_{in,m}^2} \right\} \quad (13)$$

$$\sigma_{H,j} = \frac{N_j e}{B_j} \left\{ \frac{\omega_{ce}^2}{\omega_{ce}^2+\nu_{en}^2} - \Sigma_m P_m \frac{\omega_{ci,m}^2}{\omega_{ci,m}^2+\nu_{in,m}^2} \right\} \quad (14)$$

where N_j and e are the electron density and charge and ω_{ce} is the electron gyrofrequency in the height-dependent geomagnetic field B_j. The gyrofrequency of the mth ion type is $\omega_{ci,m}$, while P_m is its relative abundance. Coefficients ν_{en} and $\nu_{in,m}$ are the electron and ion collision frequencies with neutrals. Following *Brekke and Moen* [1993], we use their ion composition and collision frequency expressions with two ion types.

The specific radio wave absorption intensities a_j at altitude h_j have been derived from the approximate Appleton-Hartree formula [e.g., *Rawer*, 1976]:

$$a_j = \frac{e^2}{2\epsilon_o m_e c \omega^2} \nu_{j,en} N_j \quad (15)$$

where $\nu_{j,en}$ is the velocity-averaged electron-neutral collision frequency for momentum transfer given, for instance, by *Mantas* [1974], while ω is the angular radio wave frequency.

4.4. Model Calculations

The model calculations have been conducted according to the following scheme. First, the magnetospheric plasma and energetic particle populations are modeled. Next an accelerating potential drop is defined. The energetic electron fluxes and energy spectra at ionospheric level are then calculated from eq. (5). The MSIS-90 model is called to define the actual profiles of neutral atmospheric composition and temperature. The specific ionization rates s_{jk} are calculated from (6) for closely spaced

Table 2a. Results of Model Calculations for Substorm Event at ~2200 UT on November 4, 1993: Thermal Magnetospheric Plasma with Maxwellian Distribution

J_j=0		V_o=0			V_o=10 kV			V_o=30 kV		
N_o, cm^{-3}	E_o, keV	A, dB	Σ_P, Ω^{-1}	Σ_H, Ω^{-1}	A, dB	Σ_P, Ω^{-1}	Σ_H, Ω^{-1}	A, dB	Σ_P, Ω^{-1}	Σ_H, Ω^{-1}
1.0	0.5	0.06	3.2	3.0	0.16	6.2	12	1.2	6.0	25
10.0	0.5	0.06	3.7	3.3	0.38	14	33	3.8	13	71
1.0	2.0	0.07	3.7	4.3	0.19	5.1	10.	1.2	5.5	21

*Here dB is the calculated absorption value in decibels referring to 30 MHz

ionospheric heights h_j and precipitating electron energy levels E_k. The ionization rate profile Q_j^* is calculated from (7) by integrating over all energies. The residual electron density profile N_o is found from the empirical model of *Friedrich and Torkar* [1983].

For steady state conditions, (11) is used to calculate the resulting electron density profile N_j, while for nonsteady conditions, (10) is integrated numerically to define N_j as a function of time. For altitudes above 110 km the constant value of the recombination coefficient given in (12) is used. For altitudes below 110 km, where the recombination coefficient depends on the actual electron density, a series of iterative calculations have been used. The recombination coefficient was derived from using the electron densities derived in the preceding step. After a few steps the results converge to give the final coupled values of N_j and α_{eff} as functions of h_j.

The height-dependent Hall and Pedersen conductivities and the specific radiowave absorption intensities can now be derived from (13) to (15) for the calculated electron density values $N_j = N_j(h)$, using the MSIS-90 atmospheric parameters, and a simple model of the geomagnetic field variations with altitude over STF. These values are finally integrated over relevant ionospheric heights h_j (60-260 km) to give the integrated Hall and Pedersen conductivities, Σ_H, Σ_P, and the total radio wave absorption A for vertically propagating cosmic noise signals. For comparison with similar events we have used 30-MHz standard frequency. The absorption intensities scale approximately as the inverse square of the frequency ratio.

In the calculations presented below we have considered two different set of models for the magnetospheric conditions above the acceleration region. In the one set there is just the thermal population of Maxwell-distributed electrons with characteristic energy E_o. These electrons are accelerated through a potential drop V_o assumed to be at an altitude of 2 R_E where $B_i/B_a \approx 16$. Accelerated electrons with resulting pitch angles within the loss cone will precipitate into the atmosphere and cause enhanced ionization. The processes are handled with the above set of formulas in (6)-(15) to derive the electron density profile, the integrated Hall and Pedersen conductivities, and the total radiowave absorption.

In an augmented models we have assumed, that some acceleration mechanism has already modified the electron distribution and has created a tail of high-energy electrons adding to the Maxwellian thermal population. The assumed spectra and intensities of the high-energy electron population are based on reported values observed from low-altitude polar-orbiting satellites and from equatorial satellites at 6-9 R_E distances [e.g., *O,Brien*, 1966; *Collis and Korth*, 1983, 1985; *Collis et al.*, 1984; *Baker et al.*, 1979, 1981, 1982] using flux spectra of the form $j(E)=j_1\exp(-E/E_1)$ with characteristic energy E_1 for the differential directional fluxes at electron energy E.

Tables 2a and 2b present a selection of computational results. Table 2a shows the thermal case (j_1=0) where we use first the above mentioned parameters for a typical magnetospheric plasma, that is, a density of N_o=1 cm^{-3}, and characteristic energy of E_o=0.5 keV (see section 4.2). In addition to using these "typical" magnetospheric electron densities and temperatures we have run the model calculations for densities an order of magnitude larger and characteristic energy a factor 4 larger, respectively. Table 2b is based on cases with an added high-energy electron population with exponential spectra of characteristic energies E_1=10, 20, and 30 keV and base flux values of $j_1=2\times10^7$, 4×10^6 and 1×10^6 cm^{-2}s^{-1}sr^{-1}keV^{-1} respectively. The accelerating voltage drop V_o has been given selected values of 0, 10 kV and 30 kV, respectively, for each case in both groups.

The above modeling has been extended to the time-varying situation for the three cases in Table 2b. We have defined a Gaussian-varying acceleration voltage impulse of maximum amplitude 30 keV and a 50% total width of 9 s and have then calculated the ionospheric absorption intensities versus time. The transit times from the acceleration region to the ionosphere have been disregarded. The results are displayed in Figure 7. The top trace represents the time-varying accelerating voltage. The lower three traces depict the calculated time-varying absorption intensities. Two main effects are seen. One is the longer ionospheric

Table 2b. Results of Model Calculations for Substorm Event at ~2200 UT on November 4, 1993: Thermal Magnetospheric Plasma and Added High-Energy Electron Population

N_o=1.0 , E_o=0.5		V_o=0			V_o=10 kV			V_o=30 kV		
J_1, fu	E_1, keV	A, dB	Σ_P, Ω^{-1}	Σ_H, Ω^{-1}	A, dB	Σ_P, Ω^{-1}	Σ_H, Ω^{-1}	A, dB	Σ_P, Ω^{-1}	Σ_H, Ω^{-1}
2.0×10^7	10	1.7	9.6	28	3.5	18	66	12.	20	130
4.0×10^6	20	4.1	7.7	27	5.9	12	48	13.	13	82
1.0×10^6	30	4.7	6.2	22	6.2	9.2	35	11.	10	55

*Here fu = flux units = cm^{-2}s^{-1}sr^{-1}keV^{-1}.

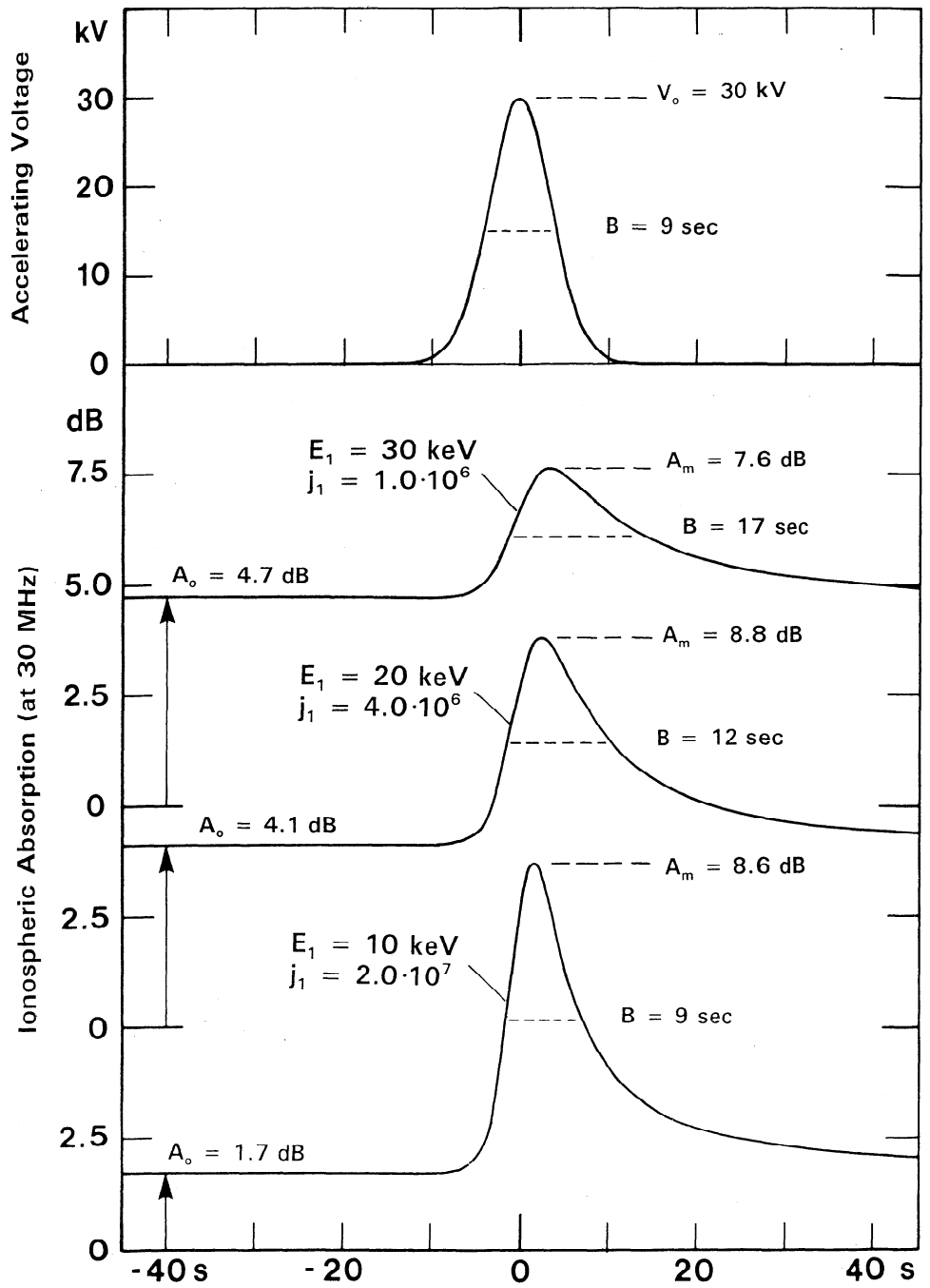

Figure 7. Time variations in absorption intensities following an impulsive (Gaussian) variation in the acceleration voltage. The three cases of Table 2b have been used for the model calculations.

response time for the more energetic spectra in the upper absorption traces. The other is the change in ratio between absorption at zero accelerating voltage and the peak absorption values at maximum acceleration. This ratio is much higher for the softer spectra at the bottom of the plot than for the harder spectra further up.

5. Discussions

This section shall discuss the implications of the modelling results, but first the realism of the model assumptions and the parameters used are commented. The calculations leading to the results presented in Tables 2a and 2b have some inherent uncertainties. The actual profiles of magnetospheric densities are not known. The mapping of the outer magnetospheric plasma region is generally very poor even on a statistical basis. One reason for this situation is the extreme complexity involved in measuring particle densities and energies in an environment of extremely diluted, very energetic plasma. Another is the sparsity of satellite observations within the region in question, that is, observations from satellites in polar orbits at altitudes from one to a few Earth radii.

For the energetic component of the electron population we rely on a combination of low-altitude satellite measurements and

high-altitude observations, for instance, from the satellites in geostationary or near-geostationary orbits. From polar orbiting satellites the occurrence of energetic "electron splash events" has been observed at latitudes beyond the usual trapping region, for instance, by *O'Brien* [1966]. He noted several cases of events with precipitation of electrons exceeding integral flux levels of 10^6 cm^{-2}s^{-1}sr^{-1} for energies greater than 40 keV. The flux values and energy spectra used in the three rows of Tables 2a and 2b correspond to fluxes of $J(E>40\text{kEV})=4.0\times10^6$, 1.0×10^7, and 8.0×10^6 cm^{-2}s^{-1}sr^{-1}, which are within range of the reported values.

Similar flux levels are also commonly seen in geostationary satellite data. In *Baker et al.* [1979, 1981, 1982] one may note, that the flux level for the $E>30$ keV channel often approaches and sometimes exceeds the level of 10^7 cm^{-2}s^{-1}sr^{-1}. The flux levels in Table 2b correspond to $J(E>30\text{ keV})=1.0\times10^7$, 1.8×10^7, and 1.1×10^7 cm^{-2}s^{-1}sr^{-1}. One should note for the comparison to geostationary data, that observed radiation spectra there are generally much harder than our rather soft model exponential spectral forms. Hence flux levels at the higher energies are much higher in the geostationary orbit than we would get with the spectra assumed for the model calculations. Considering the much higher geomagnetic latitude of our observations and noting the general softening of trapped particle spectra as one moves outward in the magnetosphere this seems reasonable.

Further, we may compare our model fluxes to the inferred fluxes in *Imhof et al.* [1984] reporting on an event that caused a 10-dB absorption spike in the South Pole 30 MHz riometer recordings. They derived an exponential spectrum for the precipitating electrons with characteristic energy of ≈40 keV and concluded that the base intensity (assuming isotropy) was $J(E>0)\approx10^9$ cm^{-2}s^{-1}sr^{-1}. Our corresponding intensities are 2.0×10^8, 8.0×10^7, and 3.0×10^7 cm^{-2}s^{-1}sr^{-1}, that is, considerably lower. Hence we have certainly not stretched the range of particle fluxes considered plausible.

A final note on the electron fluxes used for the model calculations above is a check on the "loading" of the geomagnetic field. For the field line extending from STF at invariant latitude=73.7° (L=12.7) we estimate a magnetic field intensity at the equator of ~25 nT (very uncertain). Hence the magnetic energy density is $W_{mag}=\frac{1}{2}BH\approx5\times10^{-9}$ erg/cm^3. For the three model cases in Table 2b the kinetic energy densities, $W_{kin}=(2\pi m_e)^{1/2}j_1E_1^{3/2}$ associated with the high-energy electrons are 1.0×10^{-9}, 1.1×10^{-9} and 0.5×10^{-9} erg/cm^3 respectively. The thermal (model) plasma adds 1.6×10^{-9} erg/cm^3 to the kinetic energy density. Hence the β value (W_{kin}/W_{mag}) is 0.4-0.6, that is, a moderately strong level of loading. The inferred high-energy electron fluxes by *Imhof et al.* [1984] would give an energy density of 4.3×10^{-8} erg/cm^3 which in the equatorial regions for the field line extending from South Pole ($L\approx13$) gives an unrealistic high value of $\beta\approx9$.

For the atmospheric and ionospheric model calculations there are some problem areas. The MSIS model is expected to be fairly accurate concerning the major neutral constituents, but the chemistry of the D region is complicated and there are strong influences on the reactions from minor constituents and even from cluster particles that are not included in the model at all. The calculated temperatures, furthermore, are the neutral temperatures. We have assumed that the ion and electron temperatures equal the neutral temperatures. This assumption is probably best fulfilled at D region heights where the collisions are frequent enough to keep all particles at the same temperature level. At E region heights and above the assumption is not so good. It might even be very bad for periods of magnetic activity where large ionospheric electric fields are expected to heat the electrons and ions. These uncertainties in composition and temperatures affect the recombination rates and thereby the accuracy in the derivation of the resulting electron density profiles. The possible errors may also affect the calculations of electron collision frequencies that enter both the conductance and the absorption calculations.

With these uncertainties in mind we attempt to conclude from Table 2 on the features of the modeling of the substorm on November 4, 1993. The first results are easily extracted from part a. of the table: The acceleration of the thermal magnetospheric electron population seems to be quite capable of modifying the ionospheric conductivities. We see in the first line of Table 2a that the conductivities are more than doubled in the first step using an acceleration voltage of 10 kV. As seen in the AMIE results (see Figure 3 and 4a) for the evening to midnight high-latitude substorm region, we have ionospheric potential differences of the order of 60 kV over E-W distances that correspond to the typical extent of auroral precipitation regions (~1000 km). Consequently, it seems that we have ample ground for the assumption, that the above mentioned feedback process between the ionosphere and the field-aligned potential structures will work.

The next important finding is, that the accelerated thermal magnetospheric electron fluxes are unable of producing the observed absorption intensities. The strongest case in Table 2a is that of magnetospheric densities of 10 cm^{-3}. In this case an accelerating potential of 30 kV is only capable of producing less than 4 dB of absorption at 30 MHz. One should note, that the saturating current, as defined by (3), takes a value of ~100 μA/m^2 in this case. Such currents are required by the model in order to make the potential drop rise to a high level (10-30 kV), but they are far beyond field-aligned current intensities actually observed even during highly disturbed conditions. Hence this is an unrealistic case. The increase made in the third row in characteristic energy (temperature) over the typical case considered in the first row has little effect on the calculated results. The calculated absorption values are still much to small to be comparable with the observed intensities.

Turning now to Table 2b we see that the conductivities are generally further enhanced by the added fluxes of precipitating high-energy electrons. It is not surprising that the Hall conductivities are most and the Pedersen conductivities least affected by the precipitation of the more energetic electrons since the main contributions to the Hall conductivities come from ionospheric regions lower than those that contribute most to the Pedersen conductivities.

Furthermore, we see that the high-energy electrons add considerably to the absorption intensities as one should expect since these particles penetrate down to cause enhanced ionization in the lowermost ionosphere where the electron-neutral collision frequencies increase steeply. In these cases we derive absorption intensities comparable to the observed values. The results in Table 2b, when comparing the three cases, convey the additional information that the harder fluxes with characteristic energies of 20 or 30 keV (bottom rows) are not so much influenced by the changing acceleration voltage as are the softer particles having a characteristic energy in their exponential spectre of 10 keV. This implies, that the absorption intensities produced by the more energetic particles are not easily turned on and off by even a dramatic change in the accelerating potential. The speed of change is also an important feature of the observed absorption

intensities as noted above, particularly in the discussions relating to Figures 6 and 7. The impulsive absorption spike observed at 2203:35 UT (Figure 6, middle trace) is shaped much like the E_f=10 keV model case (Figure 7, lower trace). It appears that the harder spectra (E_f=20 or 30 keV) could not possibly reproduce the observed impulsive timing.

We may further stress, referring to the first column where V_o=0, that it appears impossible to reach the observed level of absorption by the precipitation related to pitch angle scattering even in case we have a mechanism so effective that the bouncing electron population is kept isotropic as we have assumed in the calculations. The flux level required in the cases without accelerating potentials to increase the calculated absorption intensity to the observed level would load the geomagnetic field to β values much above 1 in the equatorial regions. In that case the field lines would probably be deformed and quickly eject their high-energy population. Hence the accelerating parallel electric fields are definitely needed to form a realistic model.

6. Conclusions

The data presented above have demonstrated the great potential for resolving substorm processes by combining AMIE convection analysis on a large (polar-wide) scale, but with its inherent coarse temporal and spatial resolutions (~1 min, ~ 200 km), with localized observations at the high resolution provided by the imaging riometer (~1 s, ~20 km). From the observations we have noted some very particular features, among others:

1. The substorm event at 2200 UT on November 4, 1993, occurred in the early evening sector at a quite high latitude following the poleward expansion of a preceding substorm that started 2130 UT. The general convection patterns appeared highly deformed at the time of substorm onset since the two-cell convection pattern typical of southward IMF was twisted almost 90° such that the polar antisunward convection was oriented from west to east rather than from noon to midnight. This configuration holds a significant amount of energy stored in the deformation of the outer magnetospheric fields. Part of this accumulated energy possibly feeds the observed intense substorm.

2. During the substorm onset phase the convection patterns were rapidly rotated back to their usual position. The cross-polar flow turned from dawn-dusk to noon-midnight. At the location of the key station for this study, Sdr. Strømfjord (STF), the local ionospheric potential changed by 50-60 kV during less than 10 min of the substorm event. To accomplish such changes requires large amounts of field-aligned currents. This assumption is readily verified through the AMIE calculations of the potentials and the field-aligned currents involved in the changing ionospheric patterns during the substorm.

3. The details of the temporal and spatial variations during the substorm were disclosed by the imaging riometer observations from STF that happened to be located near the center of the upward field-aligned current system at the midnight edge of the afternoon convection reversal. The imaging riometer observed a very intense ionospheric radio wave absorption event, reaching peak intensities of almost 15 dB (at 38 MHz), the largest event observed from STF during 1993.

4. The observed absorption features that probably relate to precipitation of energetic electrons was shaped like a band of width equal 30-40 km and extent of at least 350 km. The band started being E-W oriented, and rotated then through NW-SE to almost N-S at the end of the intense phase. This feature probably reflects the position of STF close to the midnight edge of the convection reversal since the precipitation-related ionization tend to drift with the general flow.

5. The absorption features were strongly variable and appeared impulsive with risetime of the order of 4-5 s, decay time of 5-7 s, and duration (within 50% level) of around 12 s. Multiple absorption impulses occurred irregularly spaced during 3 min at an average separation of 26 s.

The modeling efforts comprised calculations of the ionospheric response to precipitated energetic electrons accelerated through a field-aligned potential drop. It was assumed that the accelerated electrons were of magnetospheric origin, and from a thermal (Maxwellian) distribution without or with an added high-energy electron population with an exponential spectrum like typical trapped particle spectra observed, for instance, at the geostationary orbit and further out. The ion production rates were calculated using the Rees ionization model and the MSIS-90 model for the neutral atmospheric composition and temperatures. A simplified ion-chemistry model was used to derive the ionospheric recombination rates. These calculations have defined the added ionospheric ionization, the increased Hall and Pedersen conductivities, and the enhanced absorption of radiowaves.

The model dynamics was based on the operation of a suggested positive feedback mechanism between high-altitude field-aligned potential drops associated with upward currents, carried by magnetospheric electrons flowing down against the converging magnetic field, and the large-scale ionospheric potential structures. These horizontal potential structures are affected by the conductivity enhancements caused by precipitating energetic electrons such that positive feedback effects are possible (both up and down in amplitudes). We find that these model calculations have provided realistic results and that they support the feedback model. The model calculations gave the following results:

6. The acceleration of thermal magnetospheric electrons through a field-aligned potential drop will affect the ionospheric conductivities to an extent that makes the feedback effects feasible. The field-aligned currents needed to balance the ionospheric circuits are large enough to approach saturation whereby the parallel potential drop will increase considerably. The reduction in ionospheric potentials caused by the accomplished conductivity increases generated by the precipitated electrons may, in this case, more than account for the required potential increase along the field lines.

7. The calculated ionospheric radiowave absorption effects associated with the ionization structures generated by the one time accelerated thermal magnetospheric electrons are only up to around 1 dB for realistic cases. They are very far from being adequate to explain the absorption intensities of up to more than 10 dB observed by the imaging riometer in STF at the center of the substorm event.

8. Adding a high-energy electron population to the magnetospheric thermal population helps to provide increased absorption values. However, with flux levels limited in order not to load the magnetic field excessively in the equatorial regions, even an efficient pitch-angle scattering mechanism is inadequate of generating the precipitation needed to explain the observed absorption intensities. Field-aligned accelerating potentials are required to provide absorption values matching the observed intensities. The high-energy electrons accelerated by the field-

aligned potential structure to reach further increased energies and have changed their pitch angles to become precipitated in larger intensities have moderate additional effects on the ionospheric conductivities but large effects on the absorption intensities.

9. The best agreement with the observed absorption variability and timing was found for particle energy spectra with characteristic energies for the assumed exponential spectra of around 10 keV. The precipitation of electrons at harder spectra would be less reactive to changes in the acceleration potentials such that the observed fast absorption impulses would not be feasible. The required flux intensities are well within peak values observed in the past both by polar orbiting low-altitude satellites and geostationary satellites.

10. The impulsive character and the timing of events are compatible with a model where the time constants of the involved processes are associated with the propagation of electric signals (with Alfvénic velocities) and energetic charged particles between the ionosphere and an active acceleration region at a distance of ~1-2 R_E.

We speculate whether the energization of thermal magnetospheric electrons through repeated action of such acceleration processes may provide an adequate explanation of the high-energy electron intensities needed to accomplish the observed absorption features. To provide an effective energization process, the field-aligned acceleration voltages need to be time-varying since the electrons would otherwise just speed up and down when exposed to a stationary potential structure during their bouncing between mirror points. We suggest that the potential drop generated at intermediate altitudes by saturation of the upward current may vanish before the once downward accelerated electrons manage to again encounter the structure. The process may repeat as long as the unstably high field-aligned current intensities persists. In the observations there are indications of multiple effects since the absorption enhancements have an average separation that about matches the bounce period for energetic (10-30 keV) electrons moving along the high-latitude field lines. Hence the electrons of a bouncing cloud could repeatedly trigger the ionosphere-fieldline feed-back processes and themselves be repeatedly accelerated by the positive phase of the field-aligned potential structure. This mechanism would nicely fit the observed sequence of absorption impulses at increasing amplitude that were observed during the active phase of the redistribution of the convection patterns.

Acknowledgments. The careful operation of the DMI riometers at the extended net of observatories in Greenland including the imaging riometer at the radar station in Sdr. Strømfjord is most gratefully acknowledged. We acknowledge the use of Greenland magnetometer data made available by O. Rasmussen, DMI, the MAGIC magnetometer data supplied by C.R. Clauer from the University of Michigan, and the many other data suppliers of the magnetometer data collected for use in the AMIE processing (Knipp et al., this issue). We are in particular indebted to A. Riedley, T. Moretto, and P. Ernstrøm for their operation of the AMIE procedures that enabled the production of the very illustrative plots in Figures 3, and 4a-4d. We are further indebted to S. Kirkwood for generously supplying the PROFILE program and routines that have been a substantial part of the software used for the calculations presented above. The processing of imaging riometer data and the assistance in the reproduction efforts provided by Søren Henriksen, DMI, is greatly appreciated. The Incoherent Scatter Radar station at Sdr. Strømfjord is operated by SRI International for NSF through cooperative agreement ATM-8822560 and is also supported by the Danish Meteorological Institute. The operation of imaging riometers at Sdr. Strømfjord and Danmarkshavn has been supported by the Danish Research Council for Natural Sciences.

The editor thanks J. Fennelly and J. Lemaire for their assistance in evaluating this paper.

References

Akasofu, S.-I., The development of the auroral substorm, *Planet. Space Sci., 12*, 273, 1964.

Ahn, B.-H., R. M. Robinson, Y. Kamide, and S.-I. Akasofu, Electric conductivities, electric fields and auroral particle energy injection rate in the auroral ionosphere and their empirical relations to the horizontal magnetic disturbance, *Planet. Space Sci., 31*, 641, 1983.

Ahn, B.-H., Y. Kamide, and S.-I. Akasofu, Electrical changes of the polar ionosphere during magnetospheric substorms, *J. Geophys. Res., 91*,5737, 1986.

Baker, D., E. W. Hones Jr., R. D. Belian, P. R. Higbie, R. P. Lepping, and P. Stauning, Multiple spacecraft and correlated riometer study of magnetospheric substorm phenomena, *J. Geophys. Res.*, 87, 6121, 1982.

Baker, D., E. W. Hones Jr., P. R. Higbie, R. D. Belian, and P. Stauning, Global properties of the magnetosphere during a substorm growth phase. A case study, *J. Geophys. Res., 86*, 8941, 1981.

Baker, D., P. Stauning, E. W. Hones Jr., P. R. Higbie, and R. D. Belian, Strong electron pitch angle diffusion observed at geostationary orbit, *Geophys. Res. Lett., 6*, 205, 1979.

Banks, P. M., C. R. Chappel, and A. F. Nagy, A new model for the interaction of auroral electrons with the atmosphere: Spectral degradation, backscatter, optical emission, and ionization, *J. Geophys. Res., 79*, 1459, 1974.

Birn, J. and M. Hesse, Magnetotail instability, in *Substorms 1, Proceedings of the First International Conference on Substorms, Eur. Space Agency Spec. Publ., ESA SP-335*, 225, 1992.

Borovsky, J. E., Auroral arc thicknesses as predicted by various theories, *J. Geophys. Res., 98*, 6101, 1993.

Brekke, A., and J. Moen, Observations of high latitude ionospheric conductances, *J. Atmos. Terr. Phys., 55*, 1493, 1993.

Brüning, K., L. P. Block, G. T. Marklund, L. Eliasson, R. Pottelette, J. S. Murphree, T. A. Potemra, and S. Perraut, Viking observations above a postnoon aurora, *J. Geophys. Res., 95*, 6039, 1990.

Collis, P. N., and A. Korth, Auroral radio absorption and the westward travelling surge, *Planet. Space Sci., 31*, 1373, 1983.

Collis, P., and A. Korth, GEOS-2 observations of energetic electrons in the morning sector during auroral radio absorption events, *J. Atmos. Terr. Phys., 47*, 327, 1985.

Collis, P., J. K. Hargreaves, and A. Korth, Auroral radio absorption as an indicator of magnetospheric electrons and of conditions in the disturbed auroral *D*-region, *J. Atmos. Terr. Phys., 46*, 21, 1984.

Detrick, D. L., and T. J. Rosenberg, A phased-array radiowave imager for studies of cosmic noise absorption, *Radio Sci., 25*, 325, 1990.

Evans, D. S., The observations of a near monoenergetic flux of auroral electrons, *J. Geophys. Res., 73*, 2315, 1968.

Evans, D. S., Precipitating electron fluxes formed by a magnetic field-aligned potential difference, *J. Geophys. Res., 79*, 2853, 1974.

Feldstein, Y. I., Substorm current systems and auroral dynamics, in *Magnetospheric Substorms, Geophys. Monogr. Ser.*, vol. 64, edited by J.R Kan, T.A. Potemra, S. Kokubun, and T. Iijima, p. 29, AGU, Washington, D. C., 1991.

Fridman, M., and J. Lemaire, Relationship between auroral electron fluxes and field-aligned electric potential differences, *J. Geophys. Res., 85*, 664, 1980.

Friedrich, M., and K. M. Torkar, High latitude plasma densities and their relation to riometer absorption, *J. Atmos. Terr. Phys., 45*, 127, 1983.

Goertz, C. K., Kinetic Alfven waves on auroral field lines, *Planet. Space Sci., 32*, 1387, 1984.

Gorney, D. J., A. Clarke, D. Croley, J. Fennell, J. Luhmann, and P. Mizera, The distribution of ion beams and conics below 8000 km, *J. Geophys. Res., 86*, 83, 1981.

Hargreaves, J. K., H. J. A. Chivers, and E. Nielsen, Properties of spike events in auroral absorption, *J. Geophys. Res., 84*, 4245, 1979.

Hedin, A. E., MSIS-86 Atmospheric model, *J. Geophys. Res., 92*, 4649, 1987.

Hedin, A. E., Extension of the MSIS thermospheric model into the middle and lower atmosphere, *J. Geophys. Res., 96*, 1159, 1991.

Hoffman, R. A., and D. S. Evans, Field-aligned electron bursts at high latitudes observed by Ogo 4, *J. Geophys. Res., 73*, 6201, 1968.

Iijima, T., and T. A. Potemra, The amplitude distribution of field-aligned currents at northern high latitudes observed by Triad, *J. Geophys. Res., 81*, 2165, 1976.

Iijima, T., and T. A. Potemra, Large-scale characteristics of field-aligned currents associated with substorms, *J. Geophys. Res., 83*, 599, 1978.

Imhof, W. L., T. J. Rosenberg, L. J. Lanzerotti, J. B. Reagan, H. D.

Voss, D. W. Datlowe, J. R. Kilner, E. E. Gaines, J. Mobilia, and R. G. Joiner, A coordinated satellite and ground-based study of an intense electron spike over the southern polar cap, *J. Geophys. Res.*, *89*, 10,837, 1984.

Kan, J. R., A global magnetosphere-ionosphere coupling model of substorms, *J. Geophys. Res.*, *98*, 17,263, 1993.

Kan, J. R., and W. Sun, Substorm expansion phase caused by an intense localized convection imposed on the ionosphere, *J. Geophys. Res.*, *101*, 27,271, 1996.

Kan, J. R., R. L. Williams, and S.-I. Akasofu, A mechanism for the westward-travelling surge during substorms, *J. Geophys. Res.*, *89*, 2211, 1984.

Kan, J. R., L. Zhu, and S.-I. Akasofu, A theory of substorms.: Onset and subsidence, *J. Geophys. Res.*, *93*, 5624, 1988.

Kindel, J. M., and C. F. Kennel, Topside current instabilities, *J. Geophys. Res.*, *76*, 3055, 1971.

Kirkwood, S., SPECTRUM - A computer algoritm to derive the flux-energy spectrum of precipitating particles from EISCAT electron density profiles, *IRF Tech. Rep. 034*, Swed. Inst. of Space Phys., Kiruna, 1988.

Kirkwood, S., and A. Osepian, Quantitative studies of energetic particle precipitation using incoherent scatter radar, *J. Geomagn. Geoelectr.*, *47*, 783, 1996.

Knight, S., Parallel electric fields, *Planet. Space Sci.*, *21*, 741, 1973.

Knipp, D. J., et al., An overview of the early November 1993 geomagnetic storm. *J. Geophys. Res.*, this issue.

Lemaire, J., and M. Scherer, Ionosphere-plasma sheet field-aligned currents and parallel electric fields, *Planet. Space Sci.*, *22*, 1485, 1974.

Lemaire, J., and M. Scherer, Field aligned distribution of plasma mantle and ionospheric plasmas, *J. Atmos. Terr. Phys.*, *40*, 337, 1978.

Lin, C. S., and R. A. Hoffman, Characteristics of inverted-V events, *J. Geophys. Res.*, *84*, 1514, 1979.

Lotko, W, B. U. Ö. Sonnerup, and R. L. Lysak, Non-steady boundary layer flow including ionospheric drag and parallel electric fields, *J. Geophys. Res.*, *92*, 8635, 1987.

Lu, G., P. H. Reiff, J. L. Burch, and J. D. Winningham, On the auroral current-voltage relationship, *J. Geophys. Res.*, *96*, 3523, 1991.

Lui, A. T. Y., A synthesis model for magnetospheric substorms, in *Substorms 1, Proceedings of the First International Conference on Substorms, Eur. Space Agency Spec. Publ., ESA SP-335*, p. 43, 1992.

Lundin, R., I. Sandahl, J. Woch, and R. Elphinstone, The contribution of the boundary layer EMF to magnetospheric substorms, in *Magnetospheric Substorms, Geophys. Monogr. Ser.*, vol. 64, edited by J.R Kan, T.A. Potemra, S.Kokubun, and T. Iijima, p. 335, AGU, Washington, D.C., 1991.

Lundin, R., and D. S. Evans, Boundary layer plasmas as a source for high-latitude, early afternoon, auroral arcs, *Planet. Space Sci.*, *32*, 1389, 1985.

Lyons, L. R., Generation of large-scale regions of auroral currents, electric potentials, and precipitation by the divergence of the convection electric field, *J. Geophys. Res.*, *85*, 17, 1980.

Lyons, L. R., Formation of auroral arcs via magnetosphere-ionosphere coupling, *Rev. Geophys.*, *30*, 93, 1992.

Lyons, L. R., D. S. Evans, and R. Lundin, An observed relation between magnetic field aligned electric fields and downward electron fluxes in the vicinity of auroral forms, *J. Geophys. Res.*, *84*, 457, 1979.

Lysak, R. L., Coupling of the dynamic ionosphere to auroral flux tubes, *J. Geophys. Res.*, *91*, 7047, 1986.

Lysak, R. L., J. Grieger, and Y. Song, Fast ionospheric feedback instability and substorm onset, in *Substorms 1, Proceedings of the First International Conference on Substorms, Eur. Space Agency Spec. Publ., ESA SP-335*, p. 231, 1992.

Mantas, G. P., Electron collision frequencies and energy transfer rates, *J. Atmos. Terr. Phys.*, *36*, 1587, 1974.

McIllwain, C. E., Direct measurement of particles producing visible aurora, *J. Geophys. Res.*, *65*, 2727, 1960.

McPherron, R.L., C.T. Russell, and M.P. Aubry, Satellite studies of magnetospheric substorms on August 15, 1968. Phenomenological model for substorms, *J. Geophys. Res.*, *78*, 3131, 1973.

Murphree, J. S., and L. L. Cogger, Observations of substorm onset, in *Substorms 1, Proceedings of the First International Conference on Substorms, Eur. Space Agency Spec. Publ., ESA SP-335*, p. 207, 1992.

Nielsen, E., Dynamics and spatial scale of auroral absorption spikes associated with the substorm expansion phase, *J. Geophys. Res.*, *85*, 2092, 1980.

Nielsen, E., and W. I. Axford, Small scale auroral absorption events associated with substorms, *Nature*, *267*, 502, 1977.

O'Brien, B. J., Precipitation of electrons and protons into the atmosphere, in *Radiation Trapped in the Earth's Magnetic Field*, edited by B. M. McCormac, p. 321, D. Reidel, Norwell, Mass., 1966.

Ogawa, T., and T. Sato, New mechanism of auroral arcs, *Planet. Space Sci.*, *19*, 1393, 1971.

Pierrard, V., New model of magnetospheric current-voltage relationship, *J. Geophys. Res.*, *101*, 2669, 1996.

Pudovkin, M. I., Physics of magnetospheric substorms: A review, in *Magnetospheric Substorms, Geophys. Monogr. Ser.*, vol. 64, edited by J.R Kan, T.A. Potemra, S.Kokubun, and T. Iijima, p. 17, AGU, Washington, D. C., 1991.

Rawer, K. (Ed.), Manual on ionospheric absorption measurements, *Rep. UAG-57*, World Data Cent. A for Solar-Terrestrial Phys., Boulder, Colo., 1976.

Rees, M. H., Auroral ionization and excitation by incident energetic electrons, *Planet. Space Sci.*, *11*, 1209, 1963.

Rees, M. H., Auroral electrons, *Space Sci. Rev.*, *10*, 413, 1969.

Richmond, A. D., and Y. Kamide, Mapping electrodynamic features of the high-latitude ionosphere from localized observations: Technique, *J. Geophys. Res.*, *93*, 5741, 1988.

Roederer, J. G., *Dynamics of Geomagnetically Trapped Radiation*, Springer-Verlag Berlin, 1970.

Rostoker, G., Polar magnetic substorms, *Rev. Geophys.*, *10*, 157, 1972.

Rothwell, P. L., M. B. Silevitch, and L. P. Bloch, A model for the westward travelling surge, *J. Geophys. Res.*, *89*, 8941, 1984.

Siscoe, G. L., W. Lotko, and B. U. Ö. Sonnerup, A high-latitude, low-latitude boundary layer model of the convection current system, *J. Geophys. Res.*, *96*, 3487, 1991.

Smirnova, N., O. Ogloblina, and V. A. Vlaskov, Modelling of the lower ionosphere, *Pure Appl. Geophys.*, *127*, 353, 1988.

Sonnerup, B. U. Ö., Theory of the low latitude boundary layer, in *Proceedings of Magnetospheric Boundary Layers Conference, Eur. Space Agency Spec. Publ., ESA SP-148*, p. 395, 1979.

Stauning, P., Absorption of cosmic noise in the *E* region during electron heating events: A new class of riometer absorption events, *Geophys. Res. Lett.*, *11*, 1184, 1984.

Stauning, P., and T. J. Rosenberg, High-latitude daytime absorption spike events, *J. Geophys. Res.*, *101*, 2377, 1996.

Torkar, K. M., and M. Friedrich, Tests of an ion-chemical model in the *D*- and lower *E*-region, *J. Atmos. Terr. Phys.*, *45*, 369, 1983.

Vasyliunas, V. M., Interaction between the magnetospheric boundary layers and the ionosphere, in *Proceedings of Magnetospheric Boundary Layers Conference, Eur. Space Agency Spec. Publ., ESA SP-148*, p. 387, 1979.

Weimer, D. R., C. K. Goertz, D. A. Gurnett, N. C. Maynard, and J. L. Burch, Auroral zone electric fields from DE 1 and 2 magnetic conjunc-tions, *J. Geophys. Res.*, *90*, 7479, 1985.

Weimer, D. R., D. A. Gurnett, C. K. Goertz, J. D. Menietti, J. L. Burch, and M. Sugiura, The current-voltage relationship in auroral current sheets, *J. Geophys. Res.*, *92*, 187, 1987.

Velinov, P., N. Smirnova, and V. A. Vlascov, Hybrid quadri-ionic model of the lower ionosphere, *Adv. Space Res.*, *4*, 123, 1984.

P. Stauning, Solar-Terrestrial Physics Division, Danish Meteorological Institute, Lyngbyvej 100, DK-2100 Copenhagen Ø, Denmark. (e-mail: pst@dmi.dk)

(Received August 15, 1997; revised December 8, 1997; accepted December 8, 1997.)